

DOCUMENT CONTROL DATA - R & D

(Security classification of title, body of abstract and indexing annotation must be entered when the overall report is classified)

1. ORIGINATING ACTIVITY <i>(Corporate author)</i> Naval Research Laboratory Washington, D. C. 20375		2a. REPORT SECURITY CLASSIFICATION UNCLASSIFIED	
		2b. GROUP	
3. REPORT TITLE DESCRIPTION OF AN α - β FILTER IN CARTESIAN COORDINATES			
4. DESCRIPTIVE NOTES <i>(Type of report and inclusive dates)</i> An interim report on a continuing problem.			
5. AUTHOR(S) <i>(First name, middle initial, last name)</i> Ben H. Cantrell			
6. REPORT DATE March 21, 1973		7a. TOTAL NO. OF PAGES 50	7b. NO. OF REFS 4
8a. CONTRACT OR GRANT NO. NRL Problem R02-54		9a. ORIGINATOR'S REPORT NUMBER(S) NRL Report 7548	
b. PROJECT NO. RF 05-151-403-4010		9b. OTHER REPORT NO(S) <i>(Any other numbers that may be assigned this report)</i>	
c.			
d.			
10. DISTRIBUTION STATEMENT Approved for public release; distribution unlimited.			
11. SUPPLEMENTARY NOTES		12. SPONSORING MILITARY ACTIVITY Department of the Navy (Office of Naval Research) Arlington, Virginia 22217	
13. ABSTRACT <p>A procedure for determining the mean and covariance errors in an α-β filter operating in cartesian coordinates was found. The results obtained from this procedure were compared to an α-β filter operating in polar coordinates.</p> <p>Assuming that the input measurements in polar coordinates were Gaussian distributed, it was shown that at the output of the coordinate transformations the noise could be approximated accurately by a Gaussian distribution for typical radar data. Closed-form solutions under steady-state conditions were found for the output covariances for the polar coordinate filter and for the cartesian coordinate filter when the target is stationary. These covariances depended upon α, β, and the measurement variances. For moving targets, the cartesian coordinate filter yielded output covariances which were nonstationary. Their values depended upon α, β, measurement variances, target trajectory, target speed, and sampling time. The mean errors were discussed. Under fading conditions both the mean and covariance errors increased during the fading time.</p>			

14. KEY WORDS	LINK A		LINK B		LINK C	
	ROLE	WT	ROLE	WT	ROLE	WT
α - β tracker Track-while-scan-radar Search radar						

CONTENTS

Abstract	ii
Authorization	ii
1.0 INTRODUCTION	1
2.0 THE NOISE PROCESS	1
2.1 Polar-to-Cartesian Coordinate Transformation	1
2.2 Effect of Linear Filter	5
2.3 Cartesian-to-Polar Coordinate Transformation	7
2.4 Discussion of Results	9
3.0 FILTER DESCRIPTION	9
3.1 Filter Definition	11
3.2 Frequency Response	11
3.3 Errors Under Sinusoidal Excitation	13
3.4 Comparison of Mean Errors for Cartesian and Polar Coordinate Filters	14
3.5 Discussion of Results	17
4.0 RESPONSE TO NOISE	17
4.1 Covariance Equations	18
4.2 A Simple Stationary Solution	21
4.3 Some Nonstationary Solutions	24
4.4 Discussion of Results	28
5.0 COMPARISON OF POLAR AND CARTESIAN α - β FILTERS FOR SHORT FADE CONDITIONS AND THE TRACK HANDOFF PROBLEM	28
5.1 Mean Errors	32
5.2 Covariance Description	36
5.3 Track Handoff Problem	40
5.4 Discussion of Results	42
6.0 CONCLUSION	42
ACKNOWLEDGMENT	43
REFERENCES	43
APPENDIX — Calculation of Means and Covariances of Radar Measurements in Terms of Cartesian Coordinates ..	44

ABSTRACT

A procedure for determining the mean and covariance errors in an α - β filter operating in cartesian coordinates was found. The results obtained from this procedure were compared to an α - β filter operating in polar coordinates.

Assuming that the input measurements in polar coordinates were Gaussian distributed, it was shown that at the output of the coordinate transformations the noise could be approximated accurately by a Gaussian distribution for typical radar data. Closed-form solutions under steady-state conditions were found for the output covariances for the polar coordinate filter and for the cartesian coordinate filter when the target is stationary. These covariances depended upon α , β , and the measurement variances. For moving targets, the cartesian coordinate filter yielded output covariances which were nonstationary. Their values depended upon α , β , measurement variances, target trajectory, target speed, and sampling time. The mean errors were discussed. Under fading conditions both the mean and covariance errors increased during the fading time.

AUTHORIZATION

NRL Problem R02-54
Project RF 05-151-403-4010

Manuscript submitted January 4, 1973.

DESCRIPTION OF AN α - β FILTER IN CARTESIAN COORDINATES

1.0 INTRODUCTION

In the last several years, there has been a considerable amount of interest in automatic detection and tracking for search radar systems. Several systems exist with varying degrees of automation such as MTDS, NTDS, and the SPS-33. Others are being proposed such as the Gillfillan and APL systems for the SPS-48, the JPTDS program for the SPS-49, and the AEGIS system. Even with these efforts there is still a need to improve system performance under various conditions.

NRL Report 7434 recently studied the effects of maneuvering targets, measurement noise, false targets, and fade conditions on the ability of an α - β filter operating in polar coordinates to maintain a track (1). Even more recently NRL Report 7505 discussed the ability of this polar coordinate filter to hand off its track from the search radar to the track radar (2). In both of these reports a considerable amount of difficulty was encountered in either maintaining or handing off a track at close ranges when a polar coordinate filter was used. This was due to large range and azimuth accelerations at the close ranges. In the cartesian coordinate system these large accelerations are not encountered. However, the nonlinear transformations encountered between the two coordinates change the noise processes. It is the purpose of this report to describe analytically the α - β filter operating in cartesian coordinates and compare these results with the results of the polar coordinate filter.

Section 2.0 describes the probability densities under the coordinate system transformations. Section 3.0 describes the general characteristics of the filter and the mean errors between the predicted and true target's positions. Section 4.0 describes the covariances at the output of the filter system. Section 5.0 studies the mean and covariance errors under fading conditions and presents the results of a simulation calculating the probability of placing the beam of the tracking radar on a target using the track set up by the α - β filter. Conclusions are given in Section 6.0.

2.0 THE NOISE PROCESS

In the study of any filter it is essential to know the characteristics of the desired signals and the noise which excite the filter. The mean motion of the targets is studied in Section 3.0. The description of the noise processes proceeds as follows:

The block diagram of the filtering system is shown in Fig. 2.1. The polar coordinate radar measurements are R_m in range and θ_m in azimuth, where R_m and θ_m are assumed to be uncorrelated, Gaussian, amplitude-distributed random variables with means $\bar{\theta}_m$, \bar{R}_m

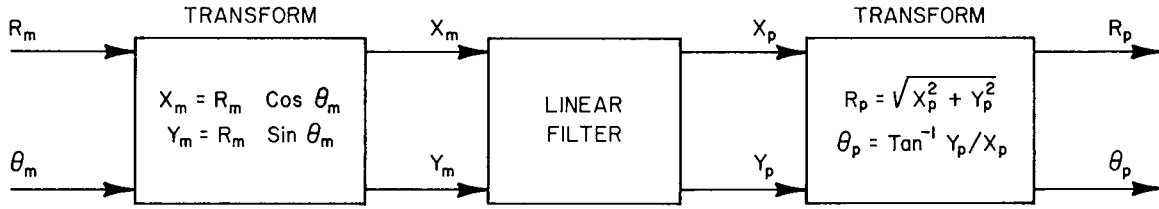


Fig. 2.1—Filter system

and variances $\sigma_{R_m}^2$, $\sigma_{\theta_m}^2$. In addition, the measurements are assumed to be independent from scan to scan of the search radar. This section is concerned with determining approximate probability densities $p(X_m, Y_m)$, $p(X_p, Y_p)$, and $p(R_p, \theta_p)$.

2.1 Polar to Cartesian Coordinate Transformation

The probability density of the polar coordinate radar measurement is

$$p(R_m, \theta_m) = \frac{1}{2\pi \sigma_{R_m} \sigma_{\theta_m}} \exp \left\{ -\frac{1}{2} \left[\frac{(R_m - \bar{R}_m)^2}{\sigma_{R_m}^2} + \frac{(\theta_m - \bar{\theta}_m)^2}{\sigma_{\theta_m}^2} \right] \right\}. \quad (2.1)$$

Contours describing constant values of the probability density function are plotted for two different cases in Figs. 2.2 and 2.3. Observing the central (10^{-8}) regions of these densities, one finds that this region appears to be a correlated Gaussian process in the (X_m, Y_m) coordinates. This observation is next investigated.

A cartesian coordinate system (p, q) is defined as shown in Figs. 2.2 and 2.3. For an arbitrary point (R_m, θ_m) in polar coordinates, the values of p and q in the p - q rectangular coordinate system are found to be

$$p = R_m [2 - \cos(\theta_m - \bar{\theta}_m)] - \bar{R}_m \quad (2.2)$$

$$q = R_m \sin(\theta_m - \bar{\theta}_m) \quad (2.3)$$

with the aid of Fig. 2.4. For cases when $(\theta_m - \bar{\theta}_m)$ is less than about 5° , Eqs. (2.2) and (2.3) can be approximated by

$$p = R_m - \bar{R}_m \quad (2.4)$$

$$q = R_m(\theta_m - \bar{\theta}_m) \quad (2.5)$$

with very little error. For example, if $\sigma_{\theta_m} = 0.5$ degrees, one would be at $10 \sigma_{\theta_m}$ or in the far tail region before the approximation begins to be significantly in error. Furthermore, if R_m does not significantly deviate from \bar{R}_m , one can further approximate Eq. (2.5) as

$$q = \bar{R}_m(\theta_m - \bar{\theta}_m). \quad (2.6)$$

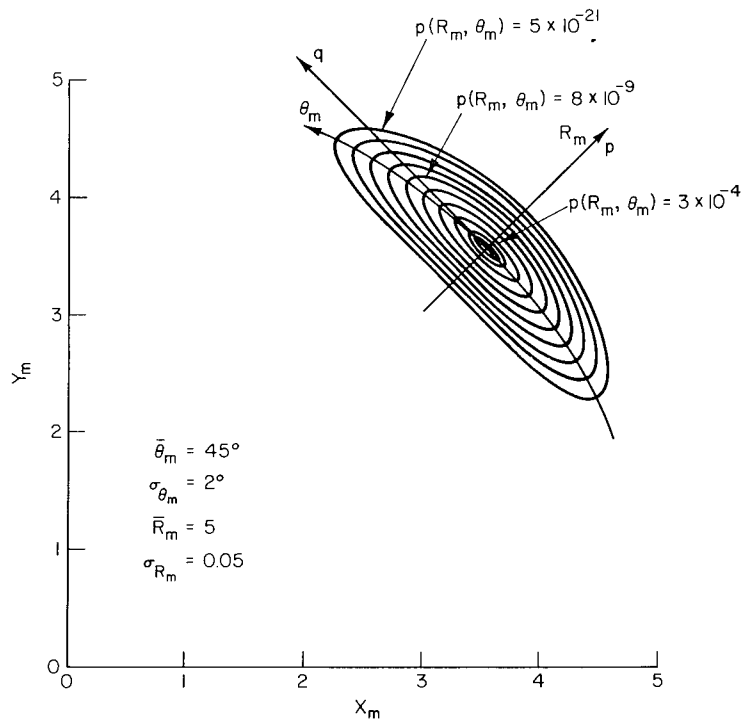


Fig. 2.2—Constant contours of $p(R_m, \theta_m)$

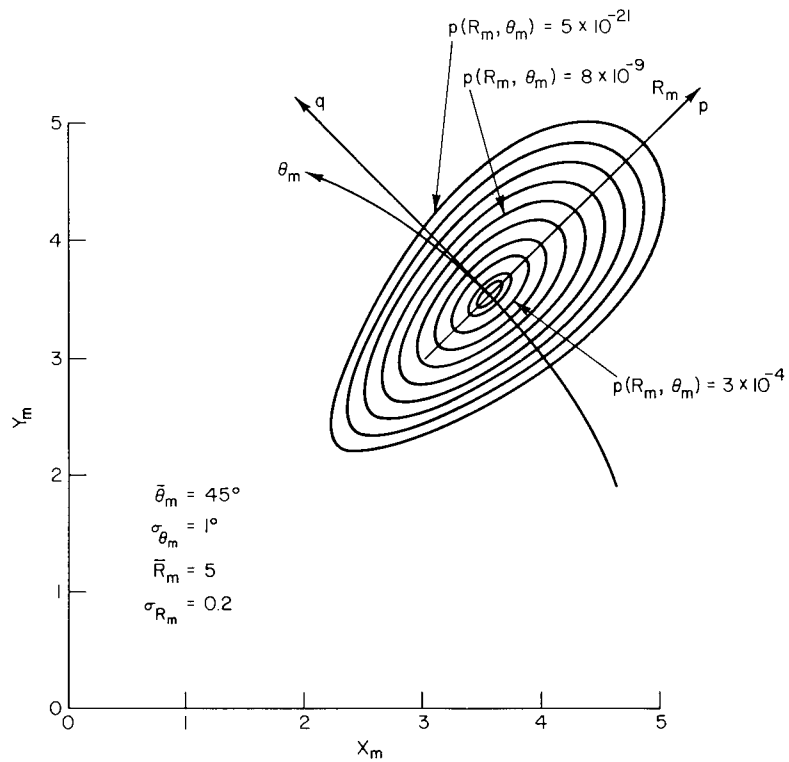


Fig. 2.3—Constant contours of $p(R_m, \theta_m)$

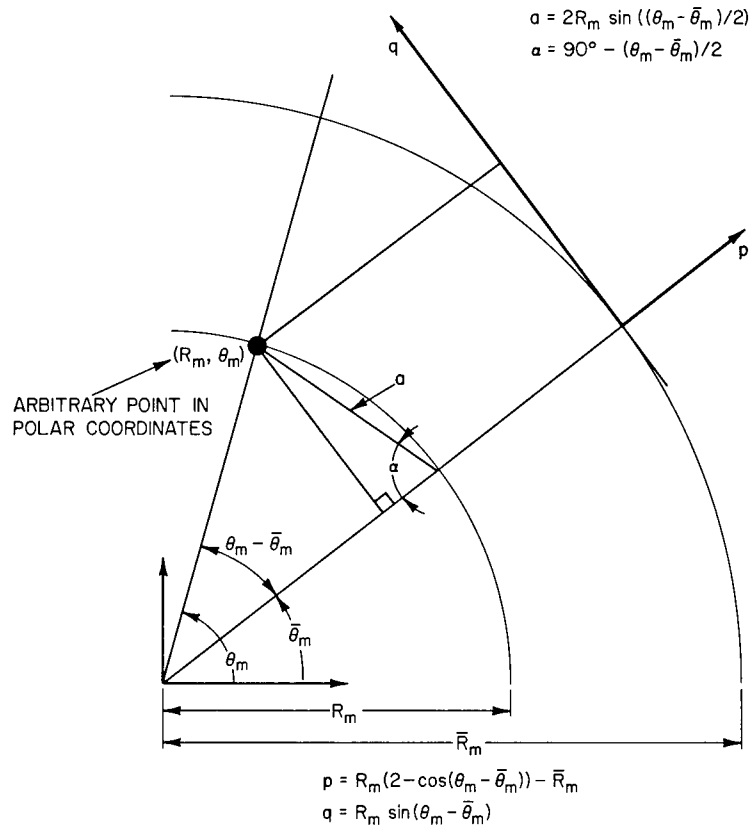


Fig. 2.4—Geometry required to compute p and q in terms of polar coordinates

For example, if $\sigma_{R_m}/\bar{R}_m = 0.01$ as would be the case for $\bar{R}_m = 4.18$ n.mi. and σ_{R_m} of 250 ft, one would be in error by 1% at one standard deviation and 5% at five standard deviations. At longer ranges the error is much less.

Equations (2.4) and (2.6) are linear transformations and therefore p and q are Gaussian distributed, at least to the extent in which the approximations are valid. By rotating the (p, q) coordinates and shifting the mean, one obtains the (X_m, Y_m) coordinates

$$X_m - \bar{X}_m = p \cos \bar{\theta}_m - q \sin \bar{\theta}_m \quad (2.7)$$

$$Y_m - \bar{Y}_m = p \sin \bar{\theta}_m + q \cos \bar{\theta}_m . \quad (2.8)$$

Again, these are linear transformations and therefore the variables (X_m, Y_m) are Gaussian distributed:

$$p(X_m, Y_m) = \frac{1}{2\pi \sigma_{x_m} \sigma_{y_m} \sqrt{1 - \rho_{x_m y_m}^2}} \times \exp \left\{ -\frac{1}{2} \left[\frac{(X_m - \bar{X}_m)^2}{\sigma_{x_m}^2} - 2\rho_{x_m y_m} \frac{(X_m - \bar{X}_m)(Y_m - \bar{Y}_m)}{\sigma_{x_m} \sigma_{y_m}} + \frac{(Y_m - \bar{Y}_m)^2}{\sigma_{y_m}^2} \right] \frac{1}{1 - \rho_{x_m y_m}^2} \right\} \quad (2.9)$$

where

$$\sigma_{x_m}^2 = \sigma_{R_m}^2 \cos^2 \bar{\theta}_m + (\bar{R}_m \sigma_{\theta_m})^2 \sin^2 \bar{\theta}_m \quad (2.10)$$

$$\sigma_{y_m}^2 = \sigma_{R_m}^2 \sin^2 \bar{\theta}_m + (\bar{R}_m \sigma_{\theta_m})^2 \cos^2 \bar{\theta}_m \quad (2.11)$$

$$\rho_{x_m y_m} = \frac{[\sigma_{R_m}^2 - (\bar{R}_m \sigma_{\theta_m})^2] \sin 2\bar{\theta}_m}{2 \sigma_{x_m} \sigma_{y_m}} \quad (2.12)$$

$$\bar{X}_m = \bar{R}_m \cos \bar{\theta}_m \quad (2.13)$$

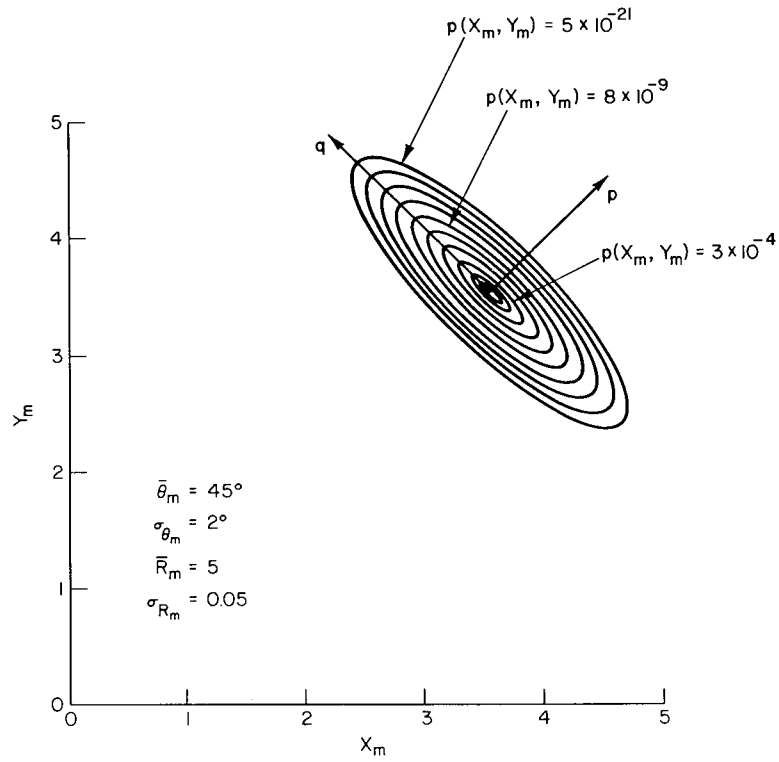
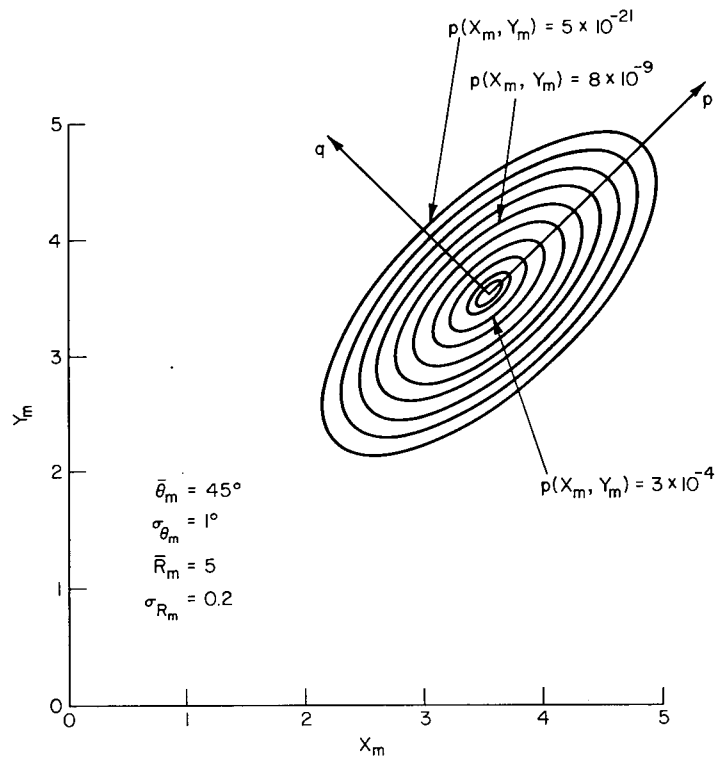
$$\bar{Y}_m = \bar{R}_m \sin \bar{\theta}_m. \quad (2.14)$$

An independent procedure for obtaining Eqs. (2.10) through (2.14) is also shown in the appendix.

The two density functions used in plotting Figs. 2.2 and 2.3 are approximated by $p(X_m, Y_m)$ shown in Eq. (2.9), and the results are shown in Figs. 2.5 and 2.6. In comparing Fig. 2.2 with 2.5 and 2.3 with 2.6, one finds that the central and near tail regions of the two densities $p(X_m, Y_m)$ and $p(R_m, \theta_m)$ are essentially the same. The approximation begins to break down in the far tail regions. However, it is the central and near tail regions which control the system. Any point in the far tail usually results in saturation or in this case no target being accepted.

2.2 Effect of Linear Filter

Since $p(X_m, Y_m)$ is essentially Gaussian, the output of a linear filter is also Gaussian distributed; i.e.,

Fig. 2.5—Constant contours of $p(X_m, Y_m)$ Fig. 2.6—Constant contours of $p(X_m, Y_m)$

$$p(X_p, Y_p) = \frac{1}{2\pi \sigma_{x_p} \sigma_{y_p} \sqrt{1 - \rho_{x_p y_p}^2}} \times \exp \left\{ -\frac{1}{2} \left[\frac{\frac{(X_p - \bar{X}_p)^2}{\sigma_{x_p}^2} - 2\rho_{x_p y_p} \frac{(X_p - \bar{X}_p)(Y_p - \bar{Y}_p)}{\sigma_{x_p} \sigma_{y_p}} + \frac{(Y_p - \bar{Y}_p)^2}{\sigma_{y_p}^2}}{1 - \rho_{x_p y_p}^2} \right] \right\}. \quad (2.15)$$

This is because the output of any filter can be written as a linear combination of the inputs, and, since the sum of Gaussian random variables is Gaussian distributed, the output of the filter is Gaussian. The means and covariances will be investigated in detail later.

2.3 Cartesian to Polar Coordinate Transformation

Contours describing constant values of the probability density function given in Eq. (2.15) are plotted for two different cases in Figs. 2.7 and 2.8. Observing these figures, it appears that the central and near tail regions of these densities are Gaussian distributed in polar coordinates. This conjecture is investigated. The (p, q) axis system is defined in Figs. 2.7 and 2.8. The $(X_p - \bar{X}_p), (Y_p - \bar{Y}_p)$ axis is rotated so as to coincide with the p - q axis. Then,

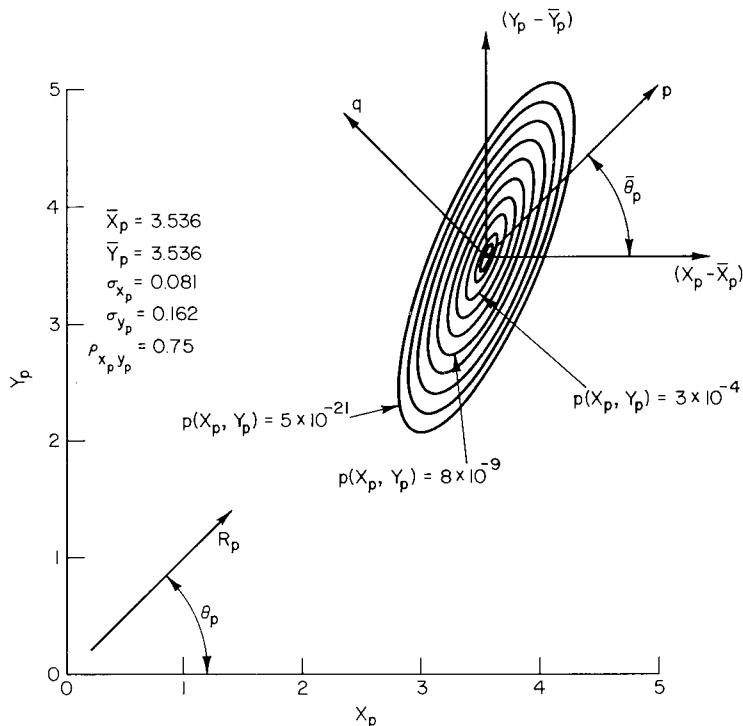
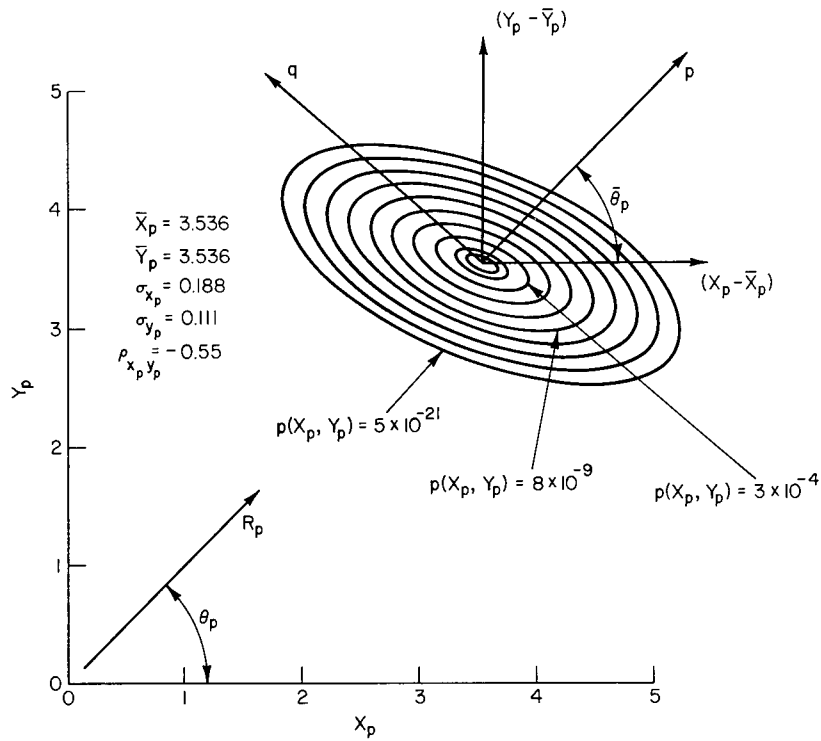


Fig. 2.7—Constant contours of $p(X_p, Y_p)$

Fig. 2.8—Constant contours of $p(X_p, Y_p)$

$$p = (X_p - \bar{X}_p) \cos \bar{\theta}_p + (Y_p - \bar{Y}_p) \sin \bar{\theta}_p \quad (2.16)$$

$$q = -(X_p - \bar{X}_p) \sin \bar{\theta}_p + (Y_p - \bar{Y}_p) \cos \bar{\theta}_p . \quad (2.17)$$

For small angular and range deviations in the coordinates (θ_p, R_p) , the approximations defined in Eq. (2.4) and (2.5) are valid:

$$R_p - \bar{R}_p = p \quad (2.18)$$

$$\bar{R}_p(\theta_p - \bar{\theta}_p) = q . \quad (2.19)$$

Combining Eqs. (2.16)-(2.19), one obtains

$$R_p = X_p \cos \bar{\theta}_p + Y_p \sin \bar{\theta}_p \quad (2.20)$$

$$\theta_p = (-X_p \sin \bar{\theta}_p + Y_p \cos \bar{\theta}_p) / \bar{R}_p . \quad (2.21)$$

Since Eqs. (2.20) and (2.21) are linear transformations on Gaussian-distributed random variables X_p and Y_p , $p(R_p, \theta_p)$ is Gaussian distributed at least over the region in which the approximation is valid:

$$p(R_p, \theta_p) = \frac{1}{2\pi \sigma_{R_p} \sigma_{\theta_p} \sqrt{1 - \rho_{R_p \theta_p}^2}} \times \exp \left\{ -\frac{1}{2} \left[\frac{(R_p - \bar{R}_p)^2}{\sigma_{R_p}^2} - 2\rho_{R_p \theta_p} \frac{(R_p - \bar{R}_p)(\theta_p - \bar{\theta}_p)}{\sigma_{R_p} \sigma_{\theta_p}} + \frac{(\theta_p - \bar{\theta}_p)^2}{\sigma_{\theta_p}^2} \right] \frac{1}{1 - \rho_{R_p \theta_p}^2} \right\}, \quad (2.22)$$

where

$$\sigma_{R_p}^2 = \sigma_{x_p}^2 \cos^2 \bar{\theta}_p + 2\sigma_{x_p} \sigma_{y_p} \rho_{x_p y_p} \cos \bar{\theta}_p \sin \bar{\theta}_p + \sigma_{y_p}^2 \sin^2 \bar{\theta}_p \quad (2.23)$$

$$\sigma_{\theta_p}^2 = \frac{\sigma_{x_p}^2 \sin^2 \bar{\theta}_p - 2\sigma_{x_p} \sigma_{y_p} \rho_{x_p y_p} \sin \bar{\theta}_p \cos \bar{\theta}_p + \sigma_{y_p}^2 \cos^2 \bar{\theta}_p}{\bar{R}_p^2} \quad (2.24)$$

$$\rho_{R_p \theta_p} = \frac{+0.5(-\sigma_{x_p}^2 + \sigma_{y_p}^2) \sin 2\bar{\theta}_p + \rho_{x_p y_p} \sigma_{x_p} \sigma_{y_p} \cos 2\bar{\theta}_p}{\sigma_{R_p} \sigma_{\theta_p} \bar{R}_p} \quad (2.25)$$

$$\bar{R}_p = \sqrt{\bar{X}_p^2 + \bar{Y}_p^2} \quad (2.26)$$

$$\bar{\theta}_p = \tan^{-1} \bar{Y}_p / \bar{X}_p. \quad (2.27)$$

The two density functions used in plotting Figs. 2.7 and 2.8 are approximated by $p(R_p, \theta_p)$ shown in Eq. (2.22), and the results are shown in Figs. 2.9 and 2.10. In comparing Fig. 2.7 with 2.9 and 2.8 with 2.10, one finds that the central and near tail regions of the two densities $p(X_p, Y_p)$ and $p(R_p, \theta_p)$ are essentially the same. Again as in Section 2.1, the approximation begins to break down in the far tail regions. However, these regions are of little interest.

2.4 Discussion of Results

The section showed that if $p(R_m, \theta_m)$ was Gaussian distributed with small variances, $p(R_p, \theta_p)$ was also Gaussian distributed over the central and near tail regions of the distribution. The means and variances after each of the coordinate transformations were found. The means and variances following the linear filter will be investigated later.

3.0 FILTER DESCRIPTION

The α - β filter is defined in this section and a few of its characteristics are shown.

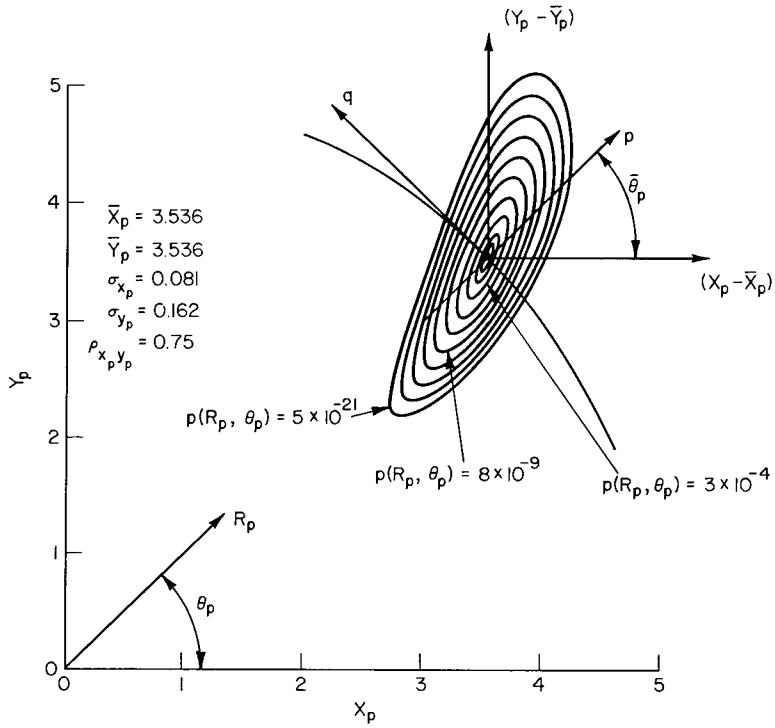


Fig. 2.9—Constant contours of $p(R_p, \theta_p)$

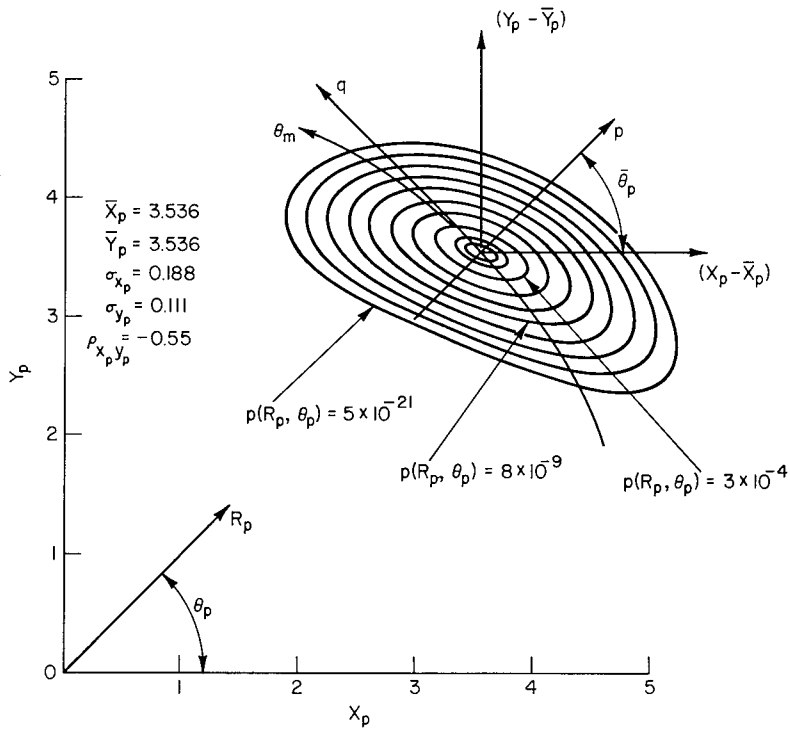


Fig. 2.10—Constant contours of $p(R_p, \theta_p)$

3.1 Filter Definition

The filter in the x coordinate is described by

$$\begin{bmatrix} X(k) \\ V_x(k) \end{bmatrix} = \begin{bmatrix} (1-\alpha) & (1-\alpha)T \\ -\beta/T & (1-\beta) \end{bmatrix} \begin{bmatrix} X(k-1) \\ V_x(k-1) \end{bmatrix} + \begin{bmatrix} \alpha \\ \beta/T \end{bmatrix} [X_m(k)] \quad (3.1)$$

$$[X_p(k+j/m)] = [1 \quad jT/m] \begin{bmatrix} X(k) \\ V_x(k) \end{bmatrix}, \quad \text{for } j = 1, \dots, m. \quad (3.2)$$

Similarly, the description in the y coordinate is

$$\begin{bmatrix} Y(k) \\ V_y(k) \end{bmatrix} = \begin{bmatrix} (1-\alpha) & (1-\alpha)T \\ -\beta/T & (1-\beta) \end{bmatrix} \begin{bmatrix} Y(k-1) \\ V_y(k-1) \end{bmatrix} + \begin{bmatrix} \alpha \\ \beta/T \end{bmatrix} [Y_m(k)] \quad (3.3)$$

$$[Y_p(k+j/m)] = [1 \quad jT/m] \begin{bmatrix} Y(k) \\ V_y(k) \end{bmatrix}, \quad \text{for } j = 1, \dots, m. \quad (3.4)$$

Since the equations are identical in each of the coordinates, it is sufficient to show a few of the characteristics in the x coordinate.

3.2 Frequency Response

Using z -transform analysis, we define the transfer functions (3) as

$$G_x = \frac{X(z)}{X_m(z)} = \frac{\alpha z \left(z + \frac{\beta - \alpha}{\alpha} \right)}{z^2 - z(2 - \alpha - \beta) + (1 - \alpha)} \quad (3.5)$$

$$G_v = \frac{V_x(z)}{X_m(z)} = \frac{(\beta/T) z (z - 1)}{z^2 - z(2 - \alpha - \beta) + (1 - \alpha)}, \quad (3.6)$$

and for $j = m$ we can define the transfer function

$$G_p = \frac{X_p(z)}{X_m(z)} = \frac{(\alpha + \beta) z \left(z - \frac{\alpha}{\alpha + \beta} \right)}{z^2 - z(2 - \alpha - \beta) + (1 - \alpha)}. \quad (3.7)$$

By placing $z = e^{j\omega T}$ into Eqs. (3.5)-(3.7), the magnitude and phase, defined as

$$\begin{array}{l} \text{magnitude} \quad |G_x| \quad |G_v| \quad |G_p| \\ \text{phase} \quad \phi_x \quad \phi_v \quad \phi_p, \end{array}$$

can be found as a function of α , β , and ωT . G_x and G_v are plotted for a given case in Fig. 3.1. This figure shows that $X(k)$ is the result of passing $X_m(k)$ through a low-pass filter, and $V_x(k)$ is the result of differentiating $X_m(k)$. The frequency of the input signal, the sampling time T , and the filter parameters α and β control the filter's response.

It is useful to place Eq. (3.5) into the form of a classical second-order system (3):

$$G_x = \frac{\alpha z \left(z + \frac{\beta - \alpha}{\alpha} \right)}{z^2 - z 2 \exp(-\xi \omega_0 T) \cos \omega_d T + \exp(-2\xi \omega_0 T)}. \quad (3.8)$$

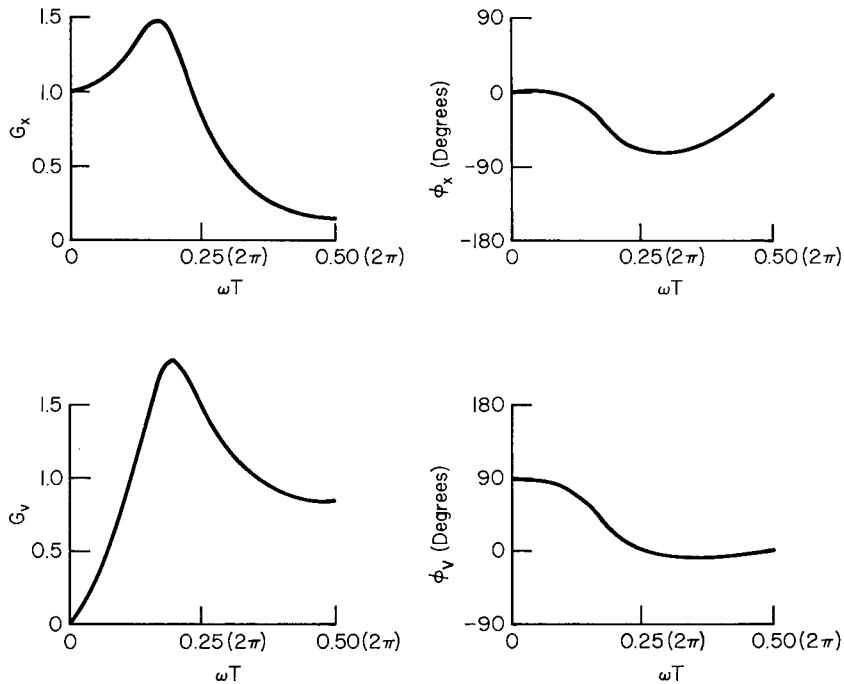


Fig. 3.1—Frequency response of α - β filter

Equating coefficients between Eqs. (3.5) and (3.8), results in

$$\alpha = 1 - e^{-2\xi \omega_0 T} \quad (3.9)$$

$$\beta = 1 + e^{-2\xi \omega_0 T} - 2 e^{-\xi \omega_0 T} \cos \omega_d T. \quad (3.10)$$

The inverse relations are

$$\xi = \frac{\ln(1/\sqrt{1-a})}{\sqrt{\left[\ln(1/\sqrt{1-\alpha})\right]^2 + \left[\cos^{-1}\left(\frac{2-\alpha-\beta}{2\sqrt{1-\alpha}}\right)\right]^2}} \quad (3.11)$$

$$\omega_d = \frac{1}{T} \cos^{-1} \frac{(2-\alpha-\beta)}{2\sqrt{1-\alpha}} \quad (3.12)$$

and

$$\omega_0 = \omega_d / \sqrt{1 - \xi^2}, \quad (3.13)$$

where ξ , ω_d , and ω_0 , are the classic damping coefficients, damped natural frequency, and natural frequency of a second-order system.

3.3 Errors Under Sinusoidal Excitation

A target having a circular motion is used to represent a turning target. The geometry is shown in Fig. 3.2. The equations of motion are

$$X_m = \bar{X}_m + |X_m| \cos \omega_0 t \quad (3.14)$$

and

$$Y_m = \bar{Y}_m + |Y_m| \sin \omega_0 t. \quad (3.15)$$

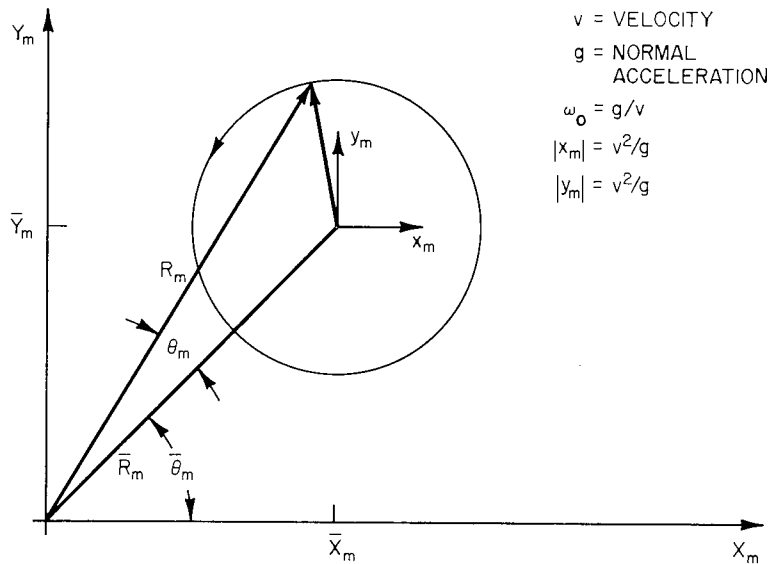


Fig. 3.2—Target geometry

The waveforms produced by the circular-motion target are passed through the filter described by Eqs. (3.1)-(3.4). Since X_m , Y_m and the operations are well defined, it is possible to obtain a closed-form solution for $R(k + j/m)$ and $\theta(k + j/m)$. However, the closed-form solutions are lengthy and involved. It is easier to simply compute numerically the results under various conditions. The error between the predicted position $X_p(k + j/m)$ and the true target position is computed as a function of time as shown in Fig. 3.3. The envelope of the peak error is sinusoidal, as would be predicted from linear system theory. In addition, the envelope of the lower peaks is almost sinusoidal and would be if $j = 0$. The error shown is valid only at the sample instants.

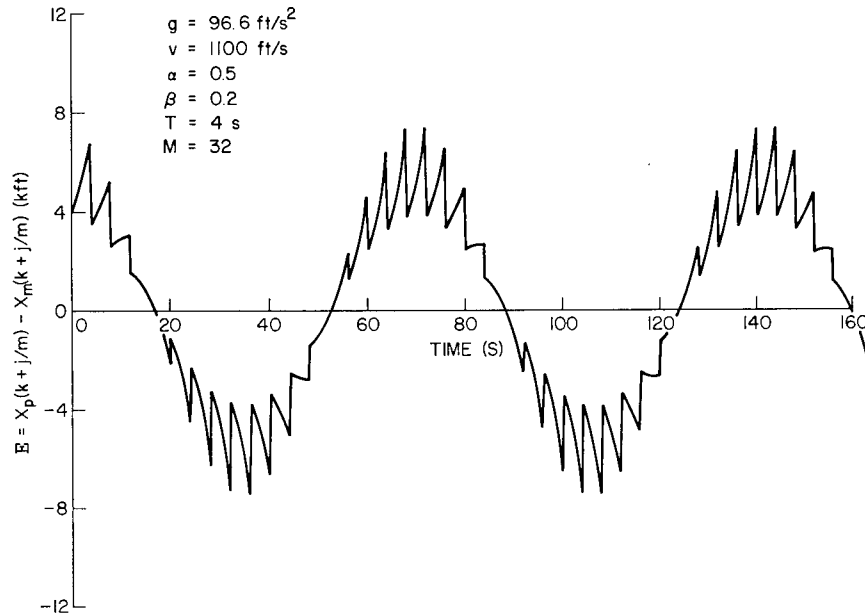


Fig. 3.3—Error between predicted and true position for a circular-motion target

The errors between the predicted and true ranges and the predicted and true azimuths are computed next. Various examples are shown in Figs. 3.4, 3.5, and 3.6. In these figures, we find that the amount of filtering affects the envelope of the peak error and the ripple errors. Although not shown, the target trajectory and the sampling time also affect the error.

3.4 Comparison of Mean Errors for Cartesian and Polar Coordinate Filters

The α - β tracker in polar coordinates is described by

$$\begin{bmatrix} R(k) \\ V_R(k) \end{bmatrix} = \begin{bmatrix} (1 - \alpha) & (1 - \alpha)T \\ -\beta/T & (1 - \beta) \end{bmatrix} \begin{bmatrix} R(k-1) \\ V_R(k-1) \end{bmatrix} + \begin{bmatrix} \alpha \\ \beta/T \end{bmatrix} [R_m(k)] \quad (3.16)$$

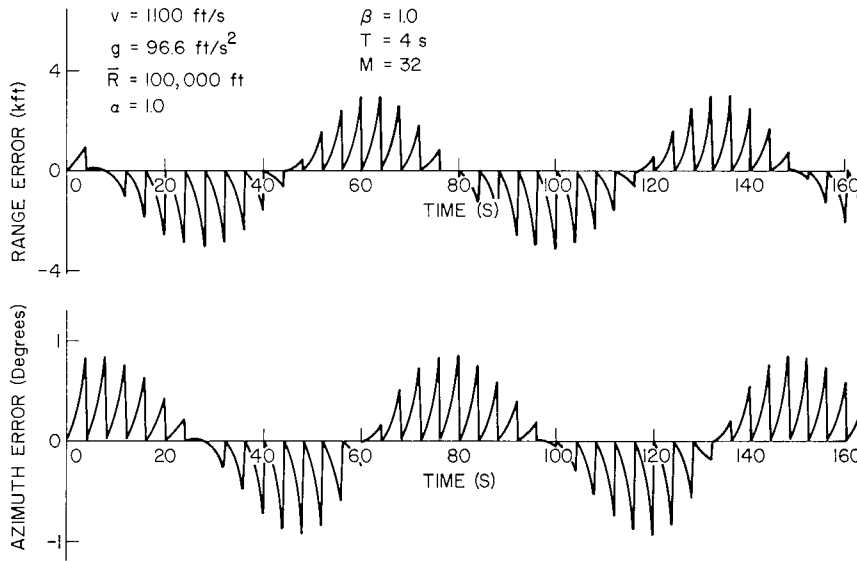


Fig. 3.4—Mean error between predicted and true positions for a circular target trajectory using an α - β tracker in cartesian coordinates

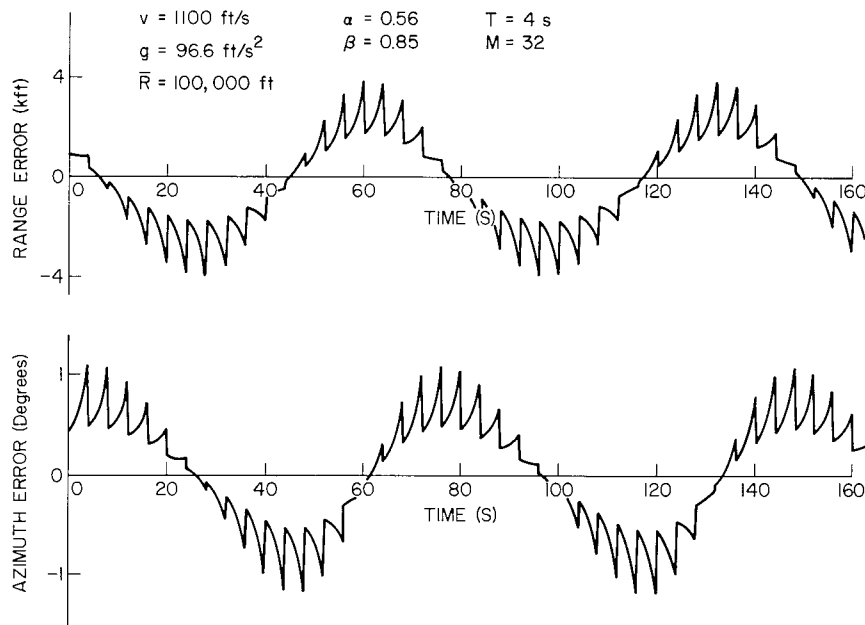


Fig. 3.5—Mean error between predicted and true position for a circular target trajectory using an α - β tracker in cartesian coordinates

$$\begin{bmatrix} \theta(k) \\ V_{\theta}(k) \end{bmatrix} = \begin{bmatrix} (1-\alpha) & (1-\alpha)T \\ -\beta/T & (1-\beta) \end{bmatrix} \begin{bmatrix} \theta(k-1) \\ V_{\theta}(k-1) \end{bmatrix} + \begin{bmatrix} \alpha \\ \beta/T \end{bmatrix} [\theta_m(k)] \quad (3.17)$$

$$R_p(k + j/m) = R(k) + (j/m) T V_R(k) \quad (3.18)$$

$$\theta_p(k + j/m) = \theta(k) + (j/m) T V_{\theta}(k) . \quad (3.19)$$

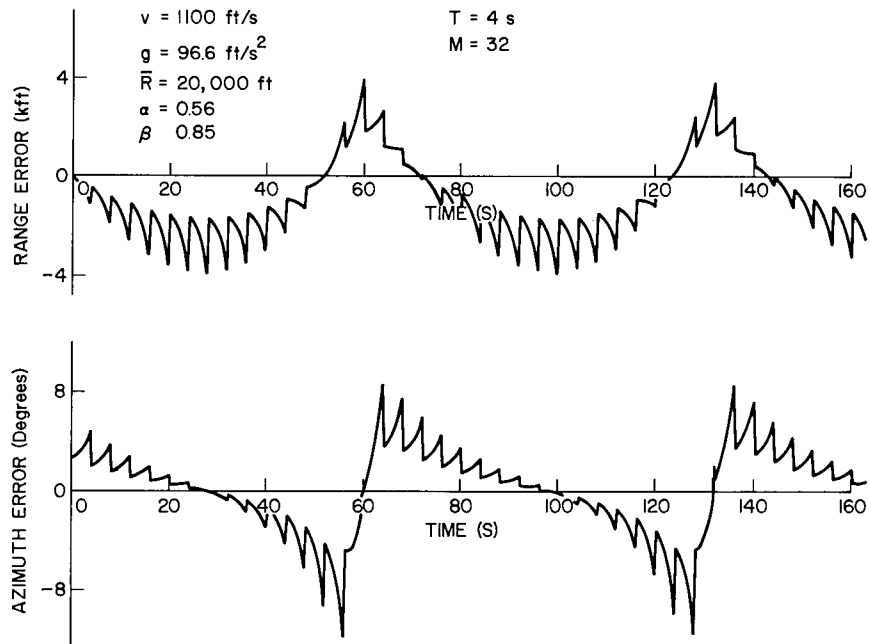


Fig. 3.6—Mean error between predicted and true position for a circular target trajectory using an α - β tracker in cartesian coordinates

For the same circular flight path as shown in Fig. 3.2, the error between the true and predicted positions in range and azimuth is computed and the results are shown in Figs. 3.7 and 3.8. As shown in these figures, the errors in the polar coordinate tracking system at the near ranges are larger than the cartesian coordinate ones. This is due to the large

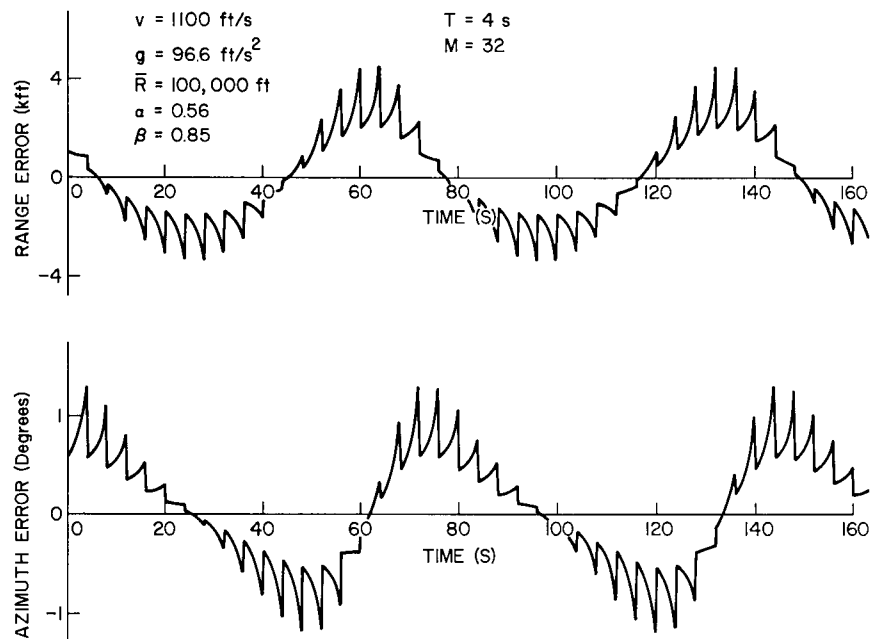


Fig. 3.7—Mean error between predicted and true positions for a circular target using an α - β tracker in polar coordinates

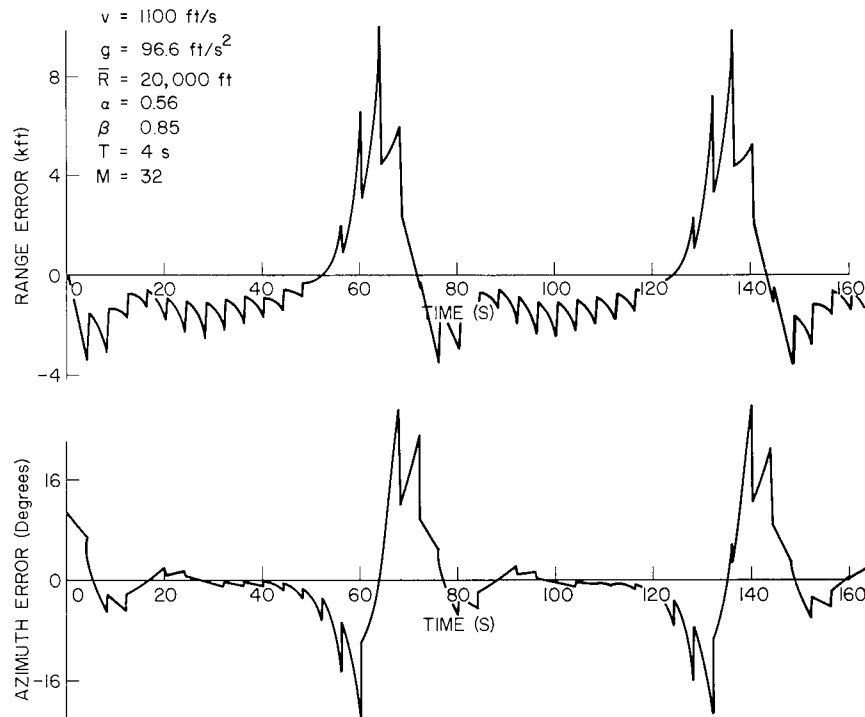


Fig. 3.8—Mean error between predicted and true positions for a circular target trajectory using an α - β tracker in polar coordinates

accelerations set up by the trajectory in polar coordinates. At the far ranges we find that the errors in either tracking system are nearly the same. This point can also be illustrated by computing the errors using both systems for a constant-velocity, straight-line flight path. For the cartesian system in steady state the error is zero. Figure 3.9 shows a typical error sequence for tracking in the polar coordinate system. Again, at the far ranges the mean tracking errors are essentially the same for either system. At short ranges the mean error in the polar system can become quite large due to the target motion and orientation with respect to the radar.

3.5 Discussion of Results

This section investigated the mean response of the filter. It was briefly described how α , β , T , target trajectory, and range affected the error between the predicted and true positions of the target. It was found that α - β trackers operating either in polar or cartesian coordinates, were essentially equivalent at the far ranges in the mean errors. The mean errors in the polar coordinate tracking system were much larger than in the cartesian coordinate system at short ranges.

4.0 RESPONSE TO NOISE

This section is concerned with computing the covariances of the noise at the output of the filter after the measurement noise described in Section 2.0 has passed through the filter described in Section 3.0.

$$\mathbf{P}(k) = \mathbf{A} \mathbf{P}(k-1) \mathbf{A}^T + \Gamma \mathbf{Q}(k) \Gamma^T, \quad (4.2)$$

where

$$\mathbf{P}(k) = \begin{bmatrix} P_{xx}(k) & P_{xv_x}(k) & P_{xy}(k) & P_{xv_y}(k) \\ P_{v_x x}(k) & P_{v_x v_x}(k) & P_{v_x y}(k) & P_{v_x v_y}(k) \\ P_{yx}(k) & P_{yv_x}(k) & P_{yy}(k) & P_{yv_y}(k) \\ P_{v_y x}(k) & P_{v_y v_x}(k) & P_{v_y y}(k) & P_{v_y v_y}(k) \end{bmatrix}$$

$$P_{xv_x} = \text{cov}(X, V_x), \text{ etc.}$$

$$\mathbf{Q}(k) = \begin{bmatrix} Q_{xx}(k) & Q_{xy}(k) \\ Q_{yx}(k) & Q_{yy}(k) \end{bmatrix}$$

$$Q_{xx}(k) = \text{cov}(X_m, X_m) = \sigma_{x_m}^2$$

$$Q_{xy}(k) = \text{cov}(X_m, Y_m) = \rho_{x_m y_m} \sigma_{x_m} \sigma_{y_m}$$

$$Q_{yy}(k) = \text{cov}(Y_m, Y_m) = \sigma_{y_m}^2.$$

The covariance equations for the filter are

$$\begin{bmatrix} P_{xx}(k) \\ P_{xv_x}(k) \\ P_{v_x v_x}(k) \end{bmatrix} = \begin{bmatrix} (1-\alpha)^2 & 2(1-\alpha)^2 T & (1-\alpha)^2 T^2 \\ -\beta(1-\alpha)/T & (1-\alpha)(1-2\beta) & (1-\alpha)(1-\beta)T \\ (\beta/T)^2 & -2\beta(1-\beta)/T & (1-\beta)^2 \end{bmatrix} \\ \times \begin{bmatrix} P_{xx}(k-1) \\ P_{xv_x}(k-1) \\ P_{v_x v_x}(k-1) \end{bmatrix} + \begin{bmatrix} \alpha^2 \\ \alpha\beta/T \\ (\beta/T)^2 \end{bmatrix} [Q_{xx}(k)] \quad (4.3)$$

$$\begin{bmatrix} P_{yy}(k) \\ P_{yv_y}(k) \\ P_{v_yv_y}(k) \end{bmatrix} = \begin{bmatrix} (1-\alpha)^2 & 2(1-\alpha)^2T & (1-\alpha)^2T^2 \\ -\beta(1-\alpha)/T & (1-\alpha)(1-2\beta) & (1-\alpha)(1-\beta)T \\ (\beta/T)^2 & -2\beta(1-\beta)/T & (1-\beta)^2 \end{bmatrix} \times \begin{bmatrix} P_{yy}(k-1) \\ P_{yv_y}(k-1) \\ P_{v_yv_y}(k-1) \end{bmatrix} + \begin{bmatrix} \alpha^2 \\ \alpha\beta/T \\ (\beta/T)^2 \end{bmatrix} [Q_{yy}(k)] \quad (4.4)$$

and

$$\begin{bmatrix} P_{yx}(k) \\ P_{v_yx}(k) \\ P_{v_xy}(k) \\ P_{v_xv_y}(k) \end{bmatrix} = \begin{bmatrix} (1-\alpha)^2 & (1-\alpha)^2T & (1-\alpha)^2T & (1-\alpha)^2T^2 \\ -\beta(1-\alpha)/T & (1-\alpha)(1-\beta) & -\beta(1-\alpha) & (1-\alpha)(1-\beta)T \\ -\beta(1-\alpha)/T & -\beta(1-\alpha) & (1-\beta)(1-\alpha) & (1-\alpha)(1-\beta)T \\ (\beta/T)^2 & (-\beta/T)(1-\beta) & (-\beta/T)(1-\beta) & (1-\beta)^2 \end{bmatrix} \times \begin{bmatrix} P_{yx}(k-1) \\ P_{v_yx}(k-1) \\ P_{v_xy}(k-1) \\ P_{v_xv_y}(k-1) \end{bmatrix} + \begin{bmatrix} \alpha^2 \\ \alpha\beta/T \\ \alpha\beta/T \\ (\beta/T)^2 \end{bmatrix} [Q_{xy}(k)] \quad (4.5)$$

Forming the covariances of Eqs. (3.2) and (3.4) yields

$$\sigma_{x_p}^2 = P_{xx}(k) + 2(j/m)TP_{xv_x}(k) + (j/m)^2T^2P_{v_xv_x}(k) \quad (4.6)$$

$$\sigma_{y_p}^2 = P_{yy}(k) + 2(j/m)TP_{yv_y}(k) + (j/m)^2T^2P_{v_yv_y}(k) \quad (4.7)$$

$$\rho_{x_p y_p} \sigma_{x_p} \sigma_{y_p} = P_{yx}(k) + (j/m)T[P_{v_yx}(k) + P_{v_xy}(k)] + (j/m)^2T^2P_{v_xv_y}(k) \quad (4.8)$$

For stationary noise inputs closed-form solutions can be found for Eqs. (4.3)-(4.5) by placing $\mathbf{P}(k+1) = \mathbf{P}(k)$ and solving the resulting algebraic equations. However, it is easier to obtain solutions by recursively solving Eqs. (4.3)-(4.5) until a steady-state solution is obtained. It is necessary to eliminate T as a parameter by substituting $\Delta y = V_y T$ and $\Delta x = V_x T$ into the original filter equations. The resulting covariance equations are of the same form as Eqs. (4.3)-(4.8) with $T = 1$. (The covariances are independent of sampling time.) Solving Eqs. (4.3)-(4.8) yields the following result:

$$F = \sigma_{x_p}^2 / Q_{xx}(k) = \sigma_{y_p}^2(k) / Q_{yy}(k) = \rho_{x_p y_p} \sigma_{x_p} \sigma_{y_p} / Q_{xy}(k). \quad (4.9)$$

For all admissible α , β , and j ; for $T = 1$; and for $F = f(\alpha, \beta, j)$.

A simple procedure for determining the solution for stationary targets is next described.

4.2 A Simple Stationary Solution

For the system shown in Fig. 2.1 the measurement means and covariances are transformed into σ_{x_m} , σ_{y_m} , $\rho_{x_m y_m}$, \bar{X}_m , \bar{Y}_m by Eqs. (2.10)-(2.14). One then computes the covariances at the output of the filter by Eqs. (4.3)-(4.8). The results $\sigma_{R_p}^2$, $\sigma_{\theta_p}^2$, $\rho_{R_p \theta_p}$, $\bar{\theta}_p$, and \bar{R}_p are then computed by Eqs. (2.23)-(2.27). If the target is stationary the input process to the filter is stationary (Eqs. (2.10)-(2.14)), and therefore the output of the filter has a stationary solution given by Eq. (4.9). In addition, $\bar{\theta}_m = \bar{\theta}_p$ and $\bar{R}_m = \bar{R}_p$. The output of the filter can then be written as

$$\sigma_{x_p}^2 = F \sigma_{R_m}^2 \cos^2 \bar{\theta}_p + F(\bar{R}_p \sigma_{\theta_m})^2 \sin^2 \bar{\theta}_p \quad (4.10)$$

$$\sigma_{y_p}^2 = F \sigma_{R_m}^2 \sin^2 \bar{\theta}_p + F(\bar{R}_p \sigma_{\theta_m})^2 \cos^2 \bar{\theta}_p \quad (4.11)$$

$$\rho_{x_p y_p} \sigma_{x_p} \sigma_{y_p} = 0.5 F \sigma_{x_m} \sigma_{y_m} \left(\sigma_{R_m}^2 - (\bar{R}_p \sigma_{\theta_m})^2 \right) \sin 2\bar{\theta}_p. \quad (4.12)$$

Substituting Eqs. (4.10)-(4.12) into Eqs. (2.23)-(2.27) results in

$$\sigma_{R_p}^2 = F \sigma_{R_m}^2 \quad (4.13)$$

$$\sigma_{\theta_p}^2 = F \sigma_{\theta_m}^2 \quad (4.14)$$

$$\rho_{R_p \theta_p} = 0 \quad (4.15)$$

$$\bar{R}_p = \bar{R}_m \quad (4.16)$$

and

$$\bar{\theta}_p = \bar{\theta}_m. \quad (4.17)$$

But this is the same solution as would have been obtained if the system shown in Fig. 4.1 had been used. The equations describing the system are

$$\begin{bmatrix} R(k) \\ V_R(k) \end{bmatrix} = \begin{bmatrix} (1-\alpha) & (1-\alpha)T \\ -\beta/T & (1-\beta) \end{bmatrix} \begin{bmatrix} R(k-1) \\ V_R(k-1) \end{bmatrix} + \begin{bmatrix} \alpha \\ \beta/T \end{bmatrix} [R_m(k)] \quad (4.18)$$

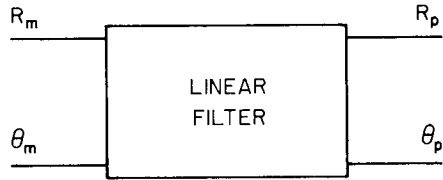


Fig. 4.1—Equivalent system to Fig. 2.1 under linear approximations used in Section 2.0

$$\begin{bmatrix} \theta(k) \\ V_\theta(k) \end{bmatrix} = \begin{bmatrix} (1-\alpha) & (1-\alpha)T \\ -\beta/T & (1-\beta) \end{bmatrix} \begin{bmatrix} \theta(k-1) \\ V_\theta(k-1) \end{bmatrix} + \begin{bmatrix} \alpha \\ \beta/T \end{bmatrix} [\theta_m(k)] \quad (4.19)$$

$$R_p(k + j/m) = R(k) + (j/m)T V_R(k) \quad (4.20)$$

and

$$\theta_p(k + j/m) = \theta(k) + (j/m)T V_\theta(k). \quad (4.21)$$

The covariance equations are formed in the same manner as before:

$$\begin{bmatrix} P_{RR}(k) \\ P_{RV_R}(k) \\ P_{V_RV_R}(k) \end{bmatrix} = \begin{bmatrix} (1-\alpha)^2 & 2(1-\alpha)^2T & (1-\alpha)^2T^2 \\ -\beta(1-\alpha)/T & (1-\alpha)(1-2\beta) & (1-\alpha)(1-\beta)T \\ (\beta/T)^2 & -2\beta(1-\beta)/T & (1-\beta)^2 \end{bmatrix} \times \begin{bmatrix} P_{RR}(k-1) \\ P_{RV_R}(k-1) \\ P_{V_RV_R}(k-1) \end{bmatrix} + \begin{bmatrix} \alpha^2 \\ \alpha\beta/T \\ (\beta/T)^2 \end{bmatrix} [Q_{RR}(k)] \quad (4.22)$$

$$\begin{bmatrix} P_{\theta\theta}(k) \\ P_{\theta V_\theta}(k) \\ P_{V_\theta V_\theta}(k) \end{bmatrix} = \begin{bmatrix} (1-\alpha)^2 & 2(1-\alpha)^2 T & (1-\alpha)^2 T^2 \\ -\beta(1-\alpha)/T & (1-\alpha)(1-2\beta) & (1-\alpha)(1-\beta)T \\ (\beta/T)^2 & -2\beta(1-\beta)/T & (1-\beta)^2 \end{bmatrix} \\
 \times \begin{bmatrix} P_{\theta\theta}(k-1) \\ P_{\theta V_\theta}(k-1) \\ P_{V_\theta V_\theta}(k-1) \end{bmatrix} + \begin{bmatrix} \alpha^2 \\ \alpha\beta/T \\ (\beta/T)^2 \end{bmatrix} [Q_{\theta\theta}(k)] \tag{4.23}$$

$$\sigma_{R_p}^2 = P_{RR}(k) + 2(j/m)T P_{RV_R}(k) + (j/m)^2 T^2 P_{V_R V_R}(k) \tag{4.24}$$

$$\sigma_{\theta_p}^2 = P_{\theta\theta}(k) + 2(j/m)T P_{\theta V_\theta}(k) + (j/m)^2 T^2 P_{V_\theta V_\theta}(k) \tag{4.25}$$

$$\rho_{R_p \theta_p} = 0 \quad \text{because } \theta_m \text{ and } R_m \text{ are uncorrelated.} \tag{4.26}$$

Since Eqs. (4.3), (4.4), (4.6), and (4.7) are identical with Eqs. (4.22)-(4.25) in form,

$$\sigma_{R_p}^2 = F \sigma_{R_m}^2 \tag{4.27}$$

$$\sigma_{\theta_p}^2 = F \sigma_{\theta_m}^2 \tag{4.28}$$

$$\rho_{R_p \theta_p} = 0 \tag{4.29}$$

$$\bar{R}_p = \bar{R}_m \tag{4.30}$$

$$\bar{\theta}_p = \bar{\theta}_m \tag{4.31}$$

Eqs. (4.13)-(4.17) are identical to Eqs. (4.27)-(4.31), a fact which shows that the system of Fig. 2.1 is the same as that of Fig. 4.1. To justify this result the following argument is given. The system shown in Fig. 2.1 is redrawn in Fig. 4.2. Recall that in Section 2.0 the polar-to-cartesian and cartesian-to-polar transformations were shown to be approximately linear over the region governing the means and covariances. The order of operation

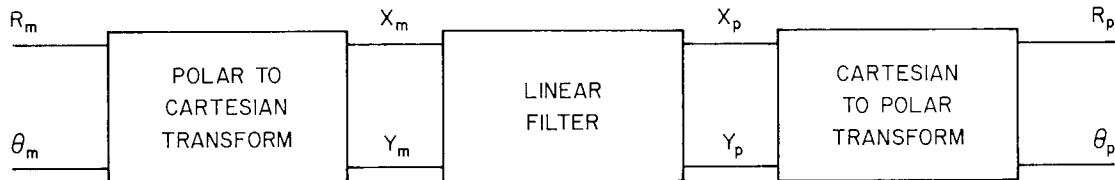


Fig. 4.2—Filter system

for linear operators can be changed, yielding the system shown in Fig. 4.3. For stationary target case the two transforms cancel, yielding Fig. 4.1.

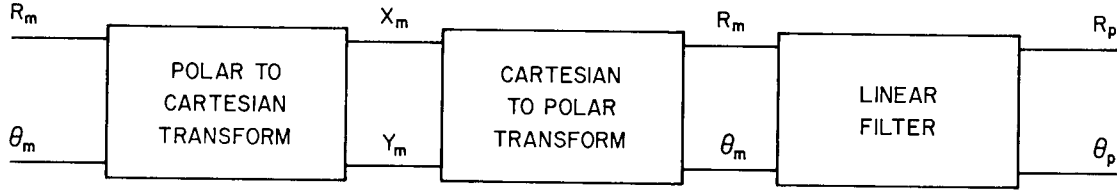


Fig. 4.3—Interchange of linear operations

The value of F can be computed as follows: $\mathbf{P}(k)$ is set equal to $\mathbf{P}(k-1)$ and the resulting algebraic equations are solved;

$$\frac{P_{RR}(k)}{\sigma_{R_m}^2} = \frac{P_{\theta\theta}(k)}{\sigma_{\theta_m}^2} = \frac{2\beta - 3\alpha\beta + 2\alpha^2}{\alpha(4 - 2\alpha - \beta)} \quad (4.32)$$

$$\frac{P_{RV_R}(k)}{\sigma_{R_m}^2} = \frac{P_{\theta V_\theta}(k)}{\sigma_{\theta_m}^2} = \frac{\beta(2\alpha - \beta)}{\alpha(4 - 2\alpha - \beta)} \quad (4.33)$$

$$\frac{P_{V_R V_R}(k)}{\sigma_{R_m}^2} = \frac{P_{V_\theta V_\theta}(k)}{\sigma_{\theta_m}^2} = \frac{\beta[2\alpha^2 - \alpha^3 + 2\beta - \alpha\beta]}{\alpha(4 - 2\alpha - \beta)} \quad (4.34)$$

$$F = \sigma_{R_p}^2 / \sigma_{R_m}^2 = \frac{P_{RR}(k)}{\sigma_{R_m}^2} + (2j/m) \frac{P_{RV_R}(k)}{\sigma_{R_m}^2} + (j/m)^2 \frac{P_{V_R V_R}(k)}{\sigma_{R_m}^2}. \quad (4.35)$$

The peak variance occurs for $j = m$. In Fig. 4.4, F is plotted vs α and β for $j = m$. Observing this figure one finds that the amount of smoothing (α and β) controls the peak noise levels. In addition, the noise varies between each scan of the search radar from k to $k = 1$. This is plotted vs j in Fig. 4.5 for large m . Observing this figure one finds that the noise is nonstationary but periodic with time under steady-state conditions.

4.3 Some Nonstationary Solutions

A target is flown at a constant velocity in a straight-line trajectory as shown in Fig. 4.6. The measurement standard deviations are assumed to be $\sigma_{R_m} = 250$ ft and $\sigma_{\theta_m} = 0.5^\circ$. Equations (2.10)-(2.14) are used to obtain $\sigma_{x_m}^2$, $\sigma_{y_m}^2$, $\rho_{x_m y_m}$, \bar{X}_m , \bar{Y}_m in terms of the measurement variances and target trajectory. Using these results with Eqs. (4.1), (4.2), and (4.3)-(4.8), we find $\sigma_{R_p}^2$, $\sigma_{\theta_p}^2$, $\rho_{R_p \theta_p}$, \bar{R}_p , and $\bar{\theta}_p$. The results for several trajectories and values of smoothing coefficients are shown in Figs. 4.7-4.12. In all cases only the envelope of the peak noise ($j = m$) is shown. The covariances will have a ripple between samples (k) and ($k+1$). In addition the dotted lines show the covariances if the target is stationary. Figures 4.7-4.12 show that the output noise processes are in general

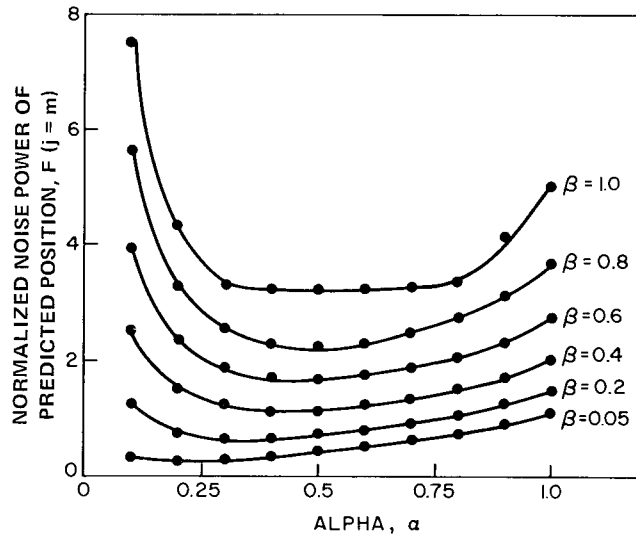


Fig. 4.4—Predicted position noise power as a function of (α, β)

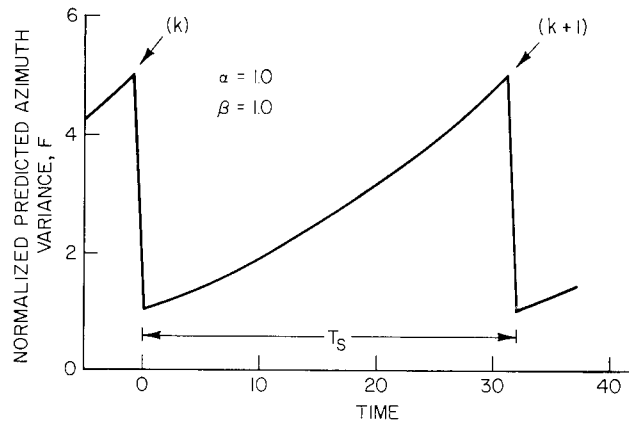
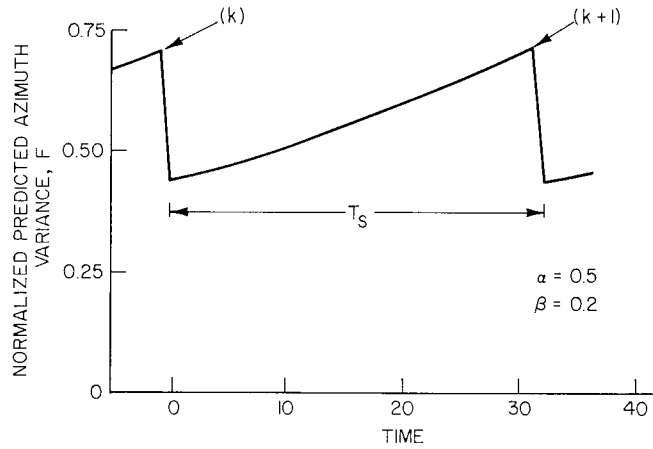


Fig. 4.5—Normalized predicted azimuth variance as a function of time

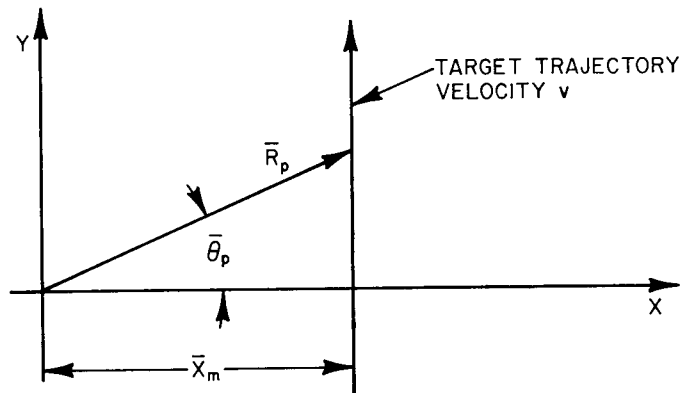


Fig. 4.6—Straight-line target trajectory

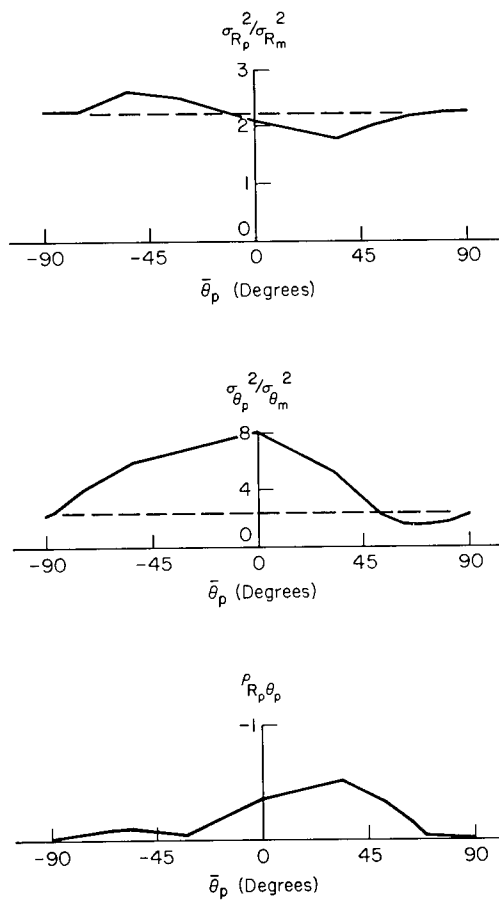


Fig. 4.7—Covariance of predicted range and azimuth for straight-line target trajectory $\bar{X}_m = 2$ n.mi., $\alpha = 0.56$, $\beta = 0.85$, $v = 2000$ ft/s

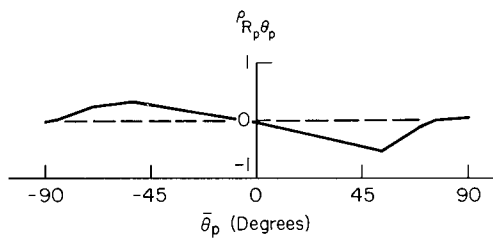
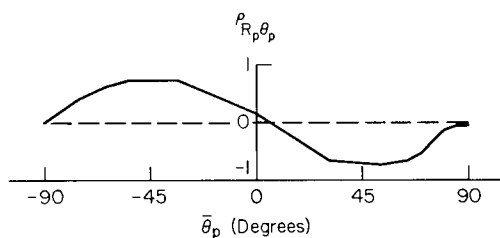
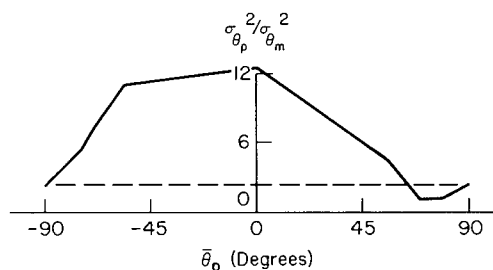
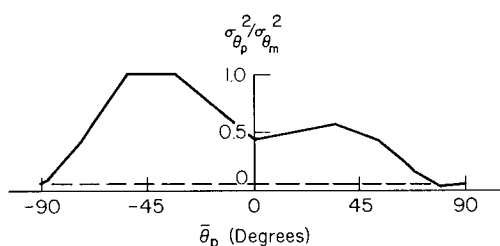
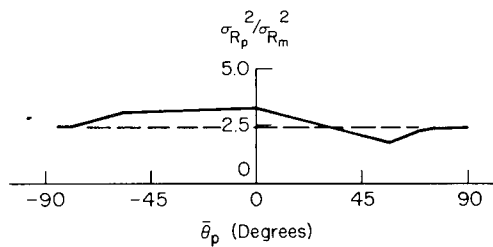
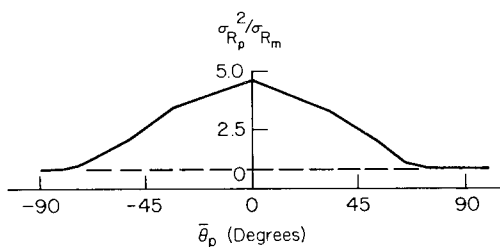


Fig. 4.8—Covariance of predicted range and azimuth for straight-line target trajectory $\bar{X}_m = 2$ n.mi., $v = 2000$ ft/s, $\alpha = 0.1$, $\beta = 0.005$

Fig. 4.9—Covariance of predicted range and azimuth for straight-line trajectory $\bar{X}_m = 2$ n.mi., $v = 2000$ ft/s, $T = 8$ s, $\alpha = 0.56$, $\beta = 0.85$

nonstationary and depend upon the target trajectory and velocity, the sampling time, and the filter parameters.

A circular flight path is flown as shown in Fig. 3.2. The covariances of the predicted range and azimuth are shown in Figs. 4.13-4.16 as a function of time for various conditions. Again only the envelope of the peak variances is plotted ($j = m$). At the far ranges or low velocities the variances of range and azimuth approach the stationary solution values, although at the long ranges it was found that the correlation did not go to zero but was a function of the turning motion. Again it is found that the covariances can be a function of target trajectory, velocity, and range; sampling time; measurement uncertainty; and filter parameters.

The effect of the faster sampler ($j = 1, \dots, m$) is shown in Fig. 4.17. Observing this figure one finds that the covariances ripple between the scan time of the search radar in a similar manner as found for the stationary solutions.

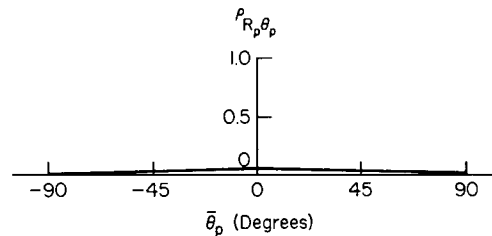
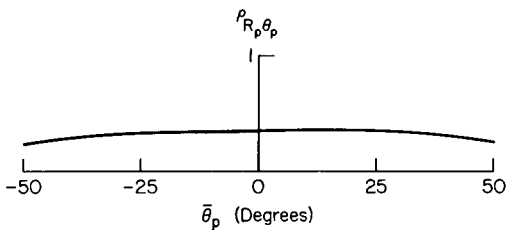
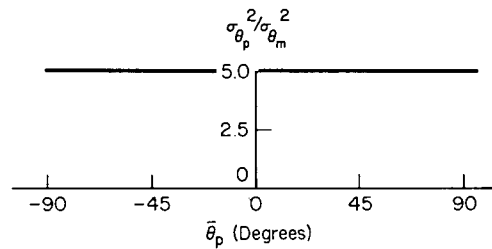
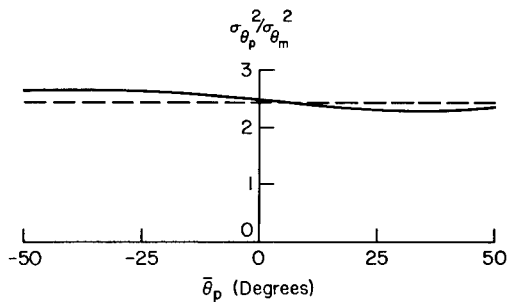
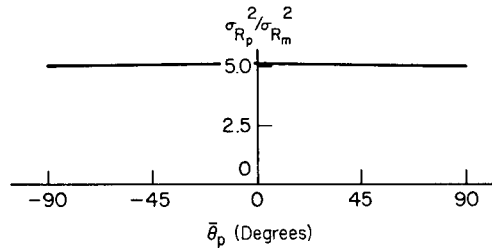
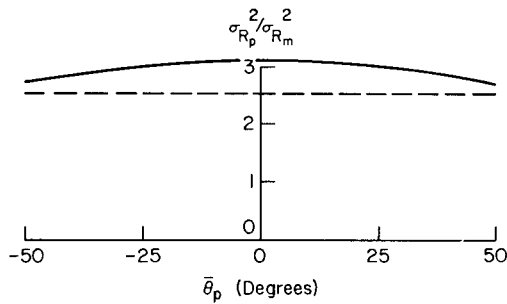


Fig. 4.10—Covariance of predicted range and azimuth for straight-line trajectory $\bar{X}_m = 30$ n.mi., $v = 2000$ ft/s, $\alpha = 0.56$, $\beta = 0.85$

Fig. 4.11—Covariance of predicted range and azimuth for straight-line target trajectory $\bar{X}_m = 30$ n.mi., $v = 500$ ft/s, $\alpha = 1.0$, $\beta = 1.0$

4.4 Discussion of Results

The covariance equations were found for both the polar and cartesian coordinate filters. A simple closed-form solution was found for the covariances in both filters when the target was stationary in space. For these cases the output correlation was zero and the output variances only depended upon α , β , and the input measurement variances. For nonstationary targets the cartesian coordinate filter yielded output covariances which depended upon α , β , input measurement variances, target trajectory and speed, and sampling time. In general the covariances increased as one came near the radar and tended to approach the stationary target solutions at the far ranges except that the correlation depended upon the turning motion.

5.0 COMPARISON OF POLAR AND CARTESIAN COORDINATE α - β FILTERS OPERATING UNDER SHORT FADE CONDITIONS

This section is concerned with evaluating the tracking performance of the polar and cartesian α - β filters for short fade conditions and for the track handoff problem. Section

Fig. 4.12—Covariance of predicted range and azimuth for straight-line trajectory flying directly at radar: $v = 2000$ ft/s, $\alpha = 0.56$, $\beta = 0.85$

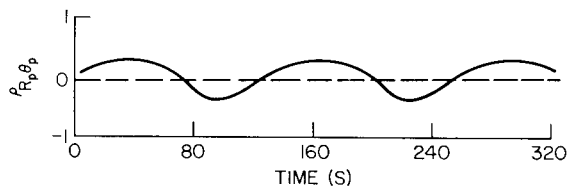
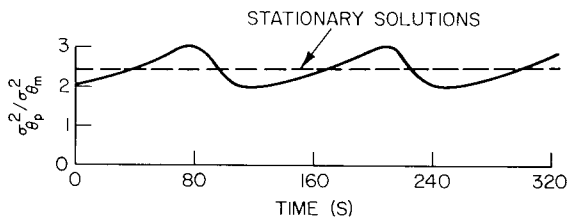
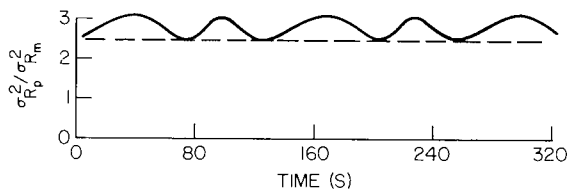
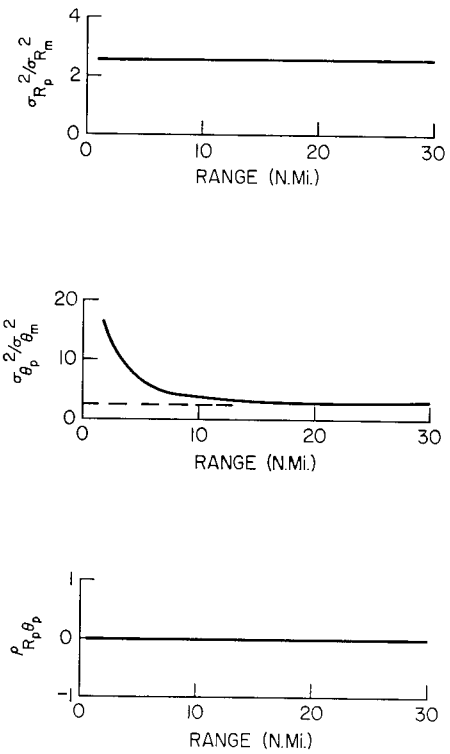


Fig. 4.13—Covariance of predicted range and azimuth for circular flight path $\bar{R}_m = 21.2$ n.mi., $\bar{\theta}_m = 45^\circ$, $v = 2000$ ft/s, 3-g turn, $\alpha = 0.56$, $\beta = 0.85$

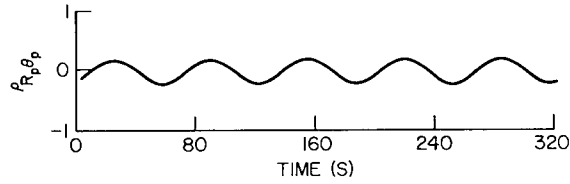
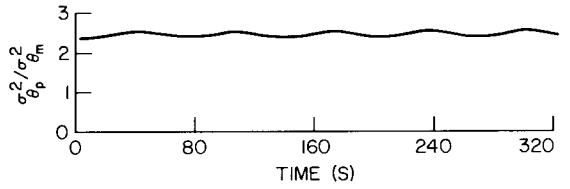
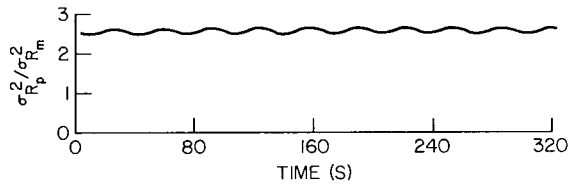


Fig. 4.14—Covariance of predicted range and azimuth for circular flight path $\bar{R}_m = 70.7$ n.mi., $\bar{\theta}_m = 45^\circ$, $v = 2000$ ft/s, 3-g turn, $\alpha = 0.56$, $\beta = 0.85$

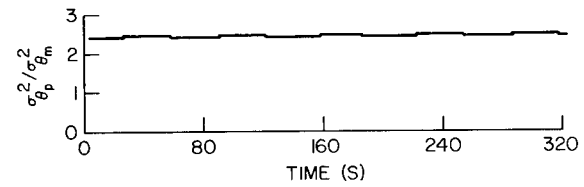
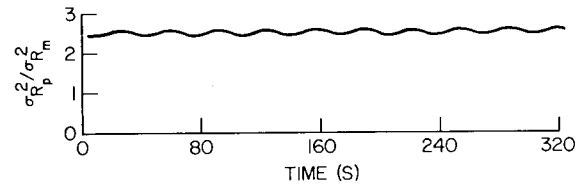


Fig. 4.15—Covariances of predicted range and azimuth for circular flight path $\bar{R}_m = 210.2$ n.mi., $\bar{\theta}_m = 45^\circ$, $v = 2000$ ft/s, 3-g turn, $\alpha = 0.56$, $\beta = 0.85$

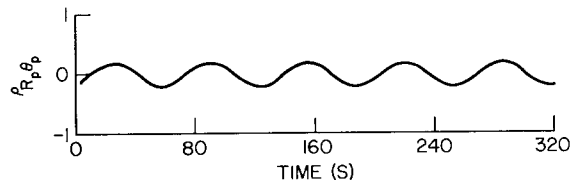


Fig. 4.16—Covariances of predicted range and azimuth for circular flight path $\bar{R}_m = 21.2$ n.mi., $\bar{\theta}_m = 45^\circ$, $v = 2000$ ft/s, 3-g turn, $\alpha = 0.1$, $\beta = 0.005$

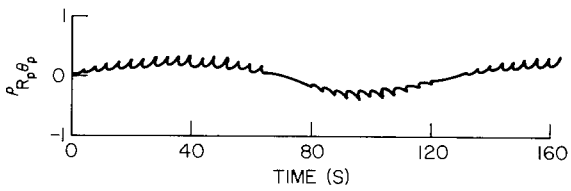
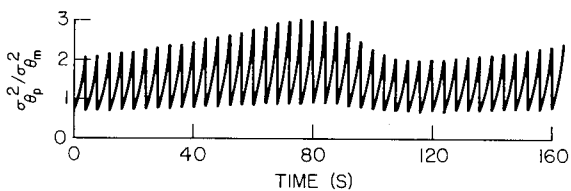
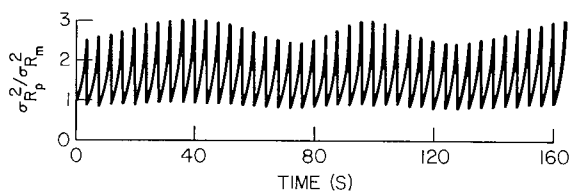
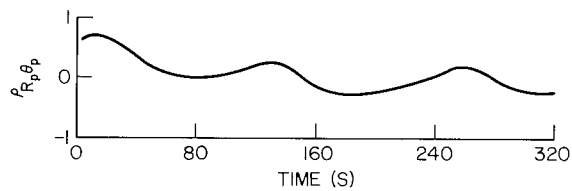
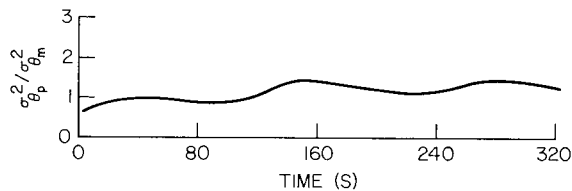
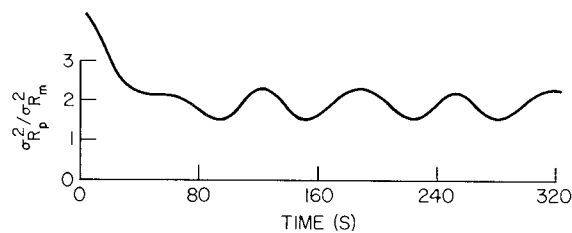


Fig. 4.17—Covariances of predicted range and azimuth for circular flight path including inter-sample ripple: $\bar{R}_m = 21.2$ n.mi., $\bar{\theta}_m = 45^\circ$, $v = 2000$ ft/s, 3-g turn, $\alpha = 0.56$, $\beta = 0.85$

5.1 describes the mean errors due to short fades, and Section 5.2 describes the effects on the covariances. Section 5.3 presents the results of the simulation on the track handoff problem.

5.1 Mean Errors

The predicted value strategy used for processing information under fading conditions is defined as follows. When a fade occurs the predicted position is set equal to the measured position. The α - β filter equations in cartesian coordinates given in Eqs. (3.1)-(3.4) reduce to

$$\begin{bmatrix} X(k) \\ V_x(k) \end{bmatrix} = \begin{bmatrix} 1 & T \\ 0 & 1 \end{bmatrix} \begin{bmatrix} X(k-1) \\ V_x(k-1) \end{bmatrix} \quad (5.1)$$

$$X_p(k + j/m) = [1 \quad jT/m] \begin{bmatrix} X(k) \\ V_x(k) \end{bmatrix} \quad (5.2)$$

$$\begin{bmatrix} Y(k) \\ V_y(k) \end{bmatrix} = \begin{bmatrix} 1 & T \\ 0 & 1 \end{bmatrix} \begin{bmatrix} Y(k-1) \\ V_y(k-1) \end{bmatrix} \quad (5.3)$$

and

$$Y_p(k + j/m) = [1 \quad jT/M] \begin{bmatrix} Y(k) \\ V_y(k) \end{bmatrix}. \quad (5.4)$$

during the period of the fade. Otherwise they are the same as before. Observing Eqs. (5.1)-(5.4), one finds that they are of the same form as Eqs. (3.1)-(3.4) except that $\alpha = \beta = 0$. Therefore Eqs. (3.1)-(3.4) can be used to represent the system under fading conditions, except that α and β are time varying between these set values and $\alpha = \beta = 0$.

In a similar manner the filter in polar coordinates is found to be represented by Eqs. (3.16)-(3.19) with time-varying coefficients of $\alpha = \beta = 0$ and the original set values of α and β corresponding to a fade and no-fade condition. Under fading conditions the polar coordinate filter moves the target along curvilinear lines at the last known radial and traverse velocities during the fade. The cartesian coordinate filter moves the target along straight lines at the last known velocity.

Several constant-velocity, straight-line target trajectories as shown in Fig. 4.6 were flown. In all cases using the cartesian coordinate filter, the mean error between the predicted and true target positions was zero under the fading sequences. By using the polar coordinate filter, the mean error between the predicted and true target azimuths was found under several conditions as shown in Figs. (5.1)-(5.4). A one in the fading sequence

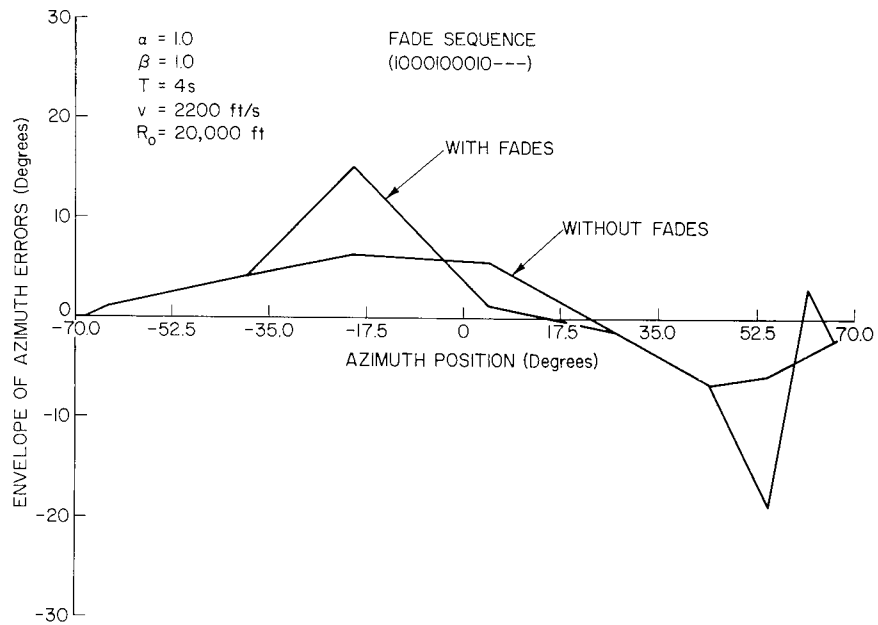


Fig. 5.1—Error between predicted and true target positions at sampling instants k ($j = m$) for straight-line target trajectory under fading conditions (tracking in polar coordinates)

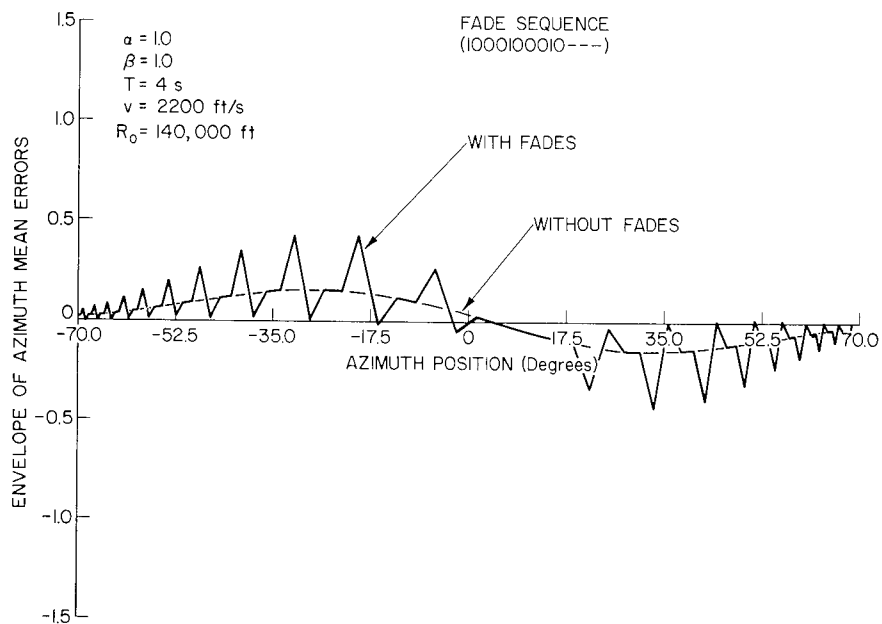


Fig. 5.2—Error between predicted and true target positions at sampling instants k ($j = m$) for straight-line target trajectory under fading conditions (tracking in polar coordinates)

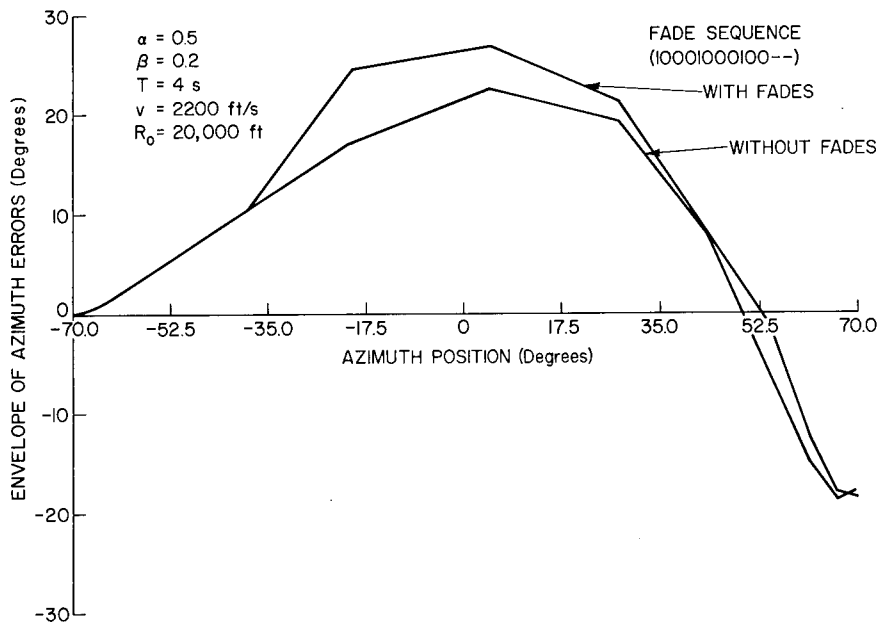


Fig. 5.3—Error between predicted and true target positions at sampling instants k ($j = m$) for straight-line target trajectory under fading conditions (tracking in polar coordinates)

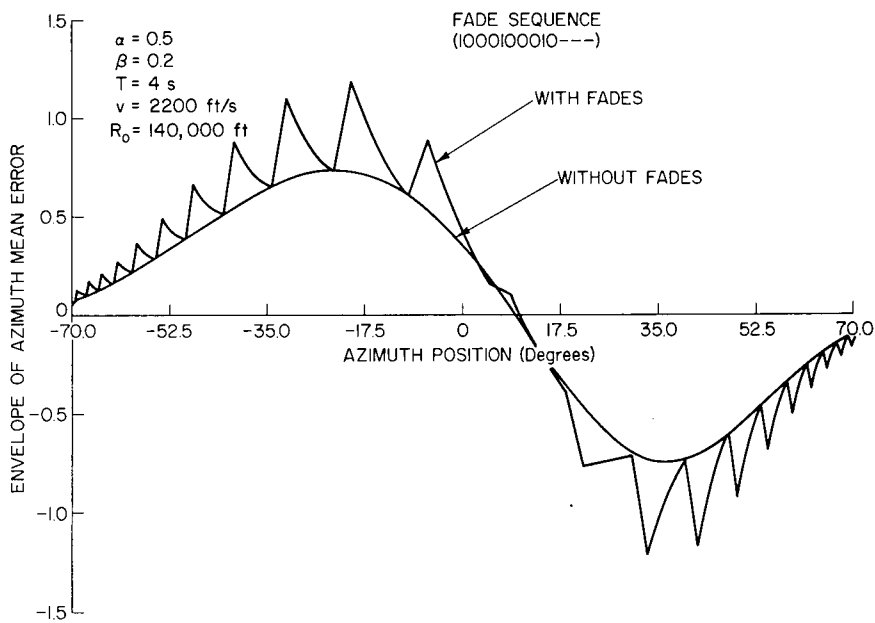


Fig. 5.4—Errors between predicted and true target position at sampling instants k ($j = m$) for straight target trajectory under fading conditions (tracking in polar coordinates)

represents a fade, whereas a zero corresponds to no fade. In all cases the envelope of the errors at sample instants ($j = m$) is shown, ignoring the ripple errors due to the faster sampler. These figures indicate that the error becomes larger as the target comes closer to the radar and when the filter uses heavier smoothing. In addition the error grows during the time the fade is present. The reason this occurs is that the target is being projected along curvilinear lines during the fades and is moving in a straight line. The error situation would be reversed if the target were moving along a traverse line rather than a straight line.

A target is flown in a circular trajectory and the mean errors between the predicted and true positions are computed for a given situation including a sequence of fades. The results are shown in Figs. 5.5 and 5.6. These figures show that at least at the farther ranges and short fading conditions the error is approximately the same using either the polar or cartesian coordinate system filter.

In general it appears that at the farther ranges where the near effect accelerations are not present in the polar coordinate system, the mean errors in either filter system under short fading conditions are nearly the same. The polar coordinate filter performs better for constant-velocity targets moving in the polar directions, whereas the cartesian coordinate filter performs better for targets moving in straight lines.

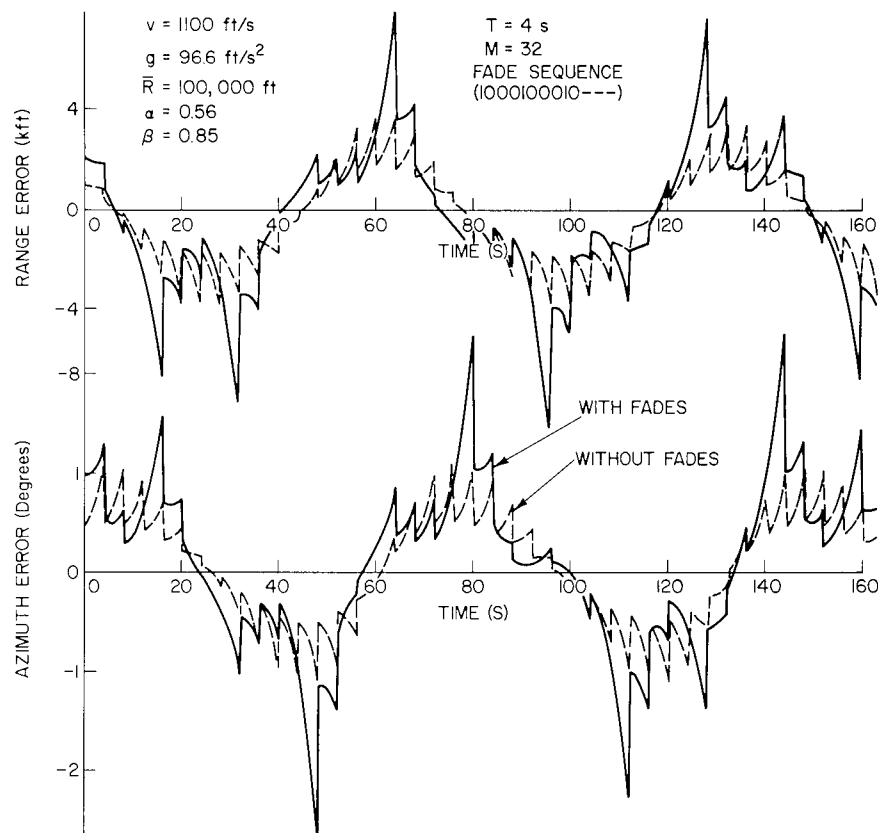


Fig. 5.5—Mean error between predicted and true positions for a circular target trajectory using an α - β filter in cartesian coordinates under fading conditions

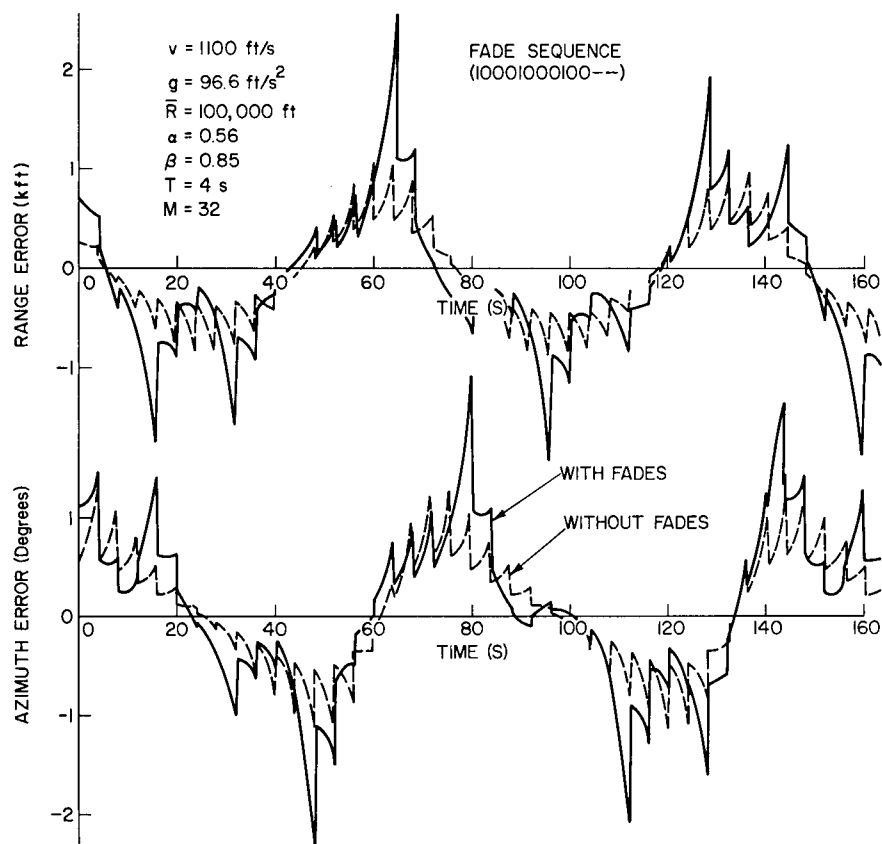


Fig. 5.6—Mean error between predicted and true positions for a circular target trajectory using an α - β filter in polar coordinates under fading conditions

5.2 Covariance Description

Under fading conditions and using the predicted position strategy as outlined in Section 5.1, the covariances are described in the same manner as in Section 4.0 except that when a fade occurs α and β are set equal to zero. A constant-velocity target is flown in a straight line and the covariances are computed under a fading condition for two cases as shown in Figs. 5.7 and 5.8. The cartesian coordinate filter is used and the envelope of the covariances ($j = m$) is shown. The covariances increase during a fading condition. The covariances were computed using the polar coordinate filter and are shown in Fig. 5.9. Unlike the cartesian coordinate filter, in this case the covariances are independent of target trajectory, speed, and sampling time.

A circular flight path is flown and the covariances are computed using the polar and cartesian coordinate filters. The results are shown in Figs. 5.10-5.12, which show that the covariances increase as the target fades.

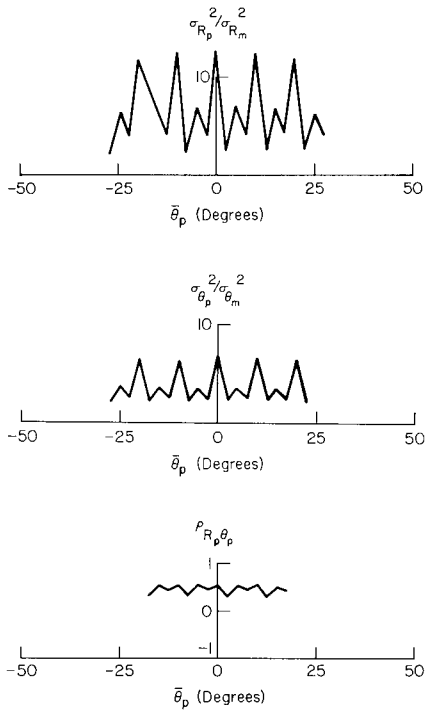
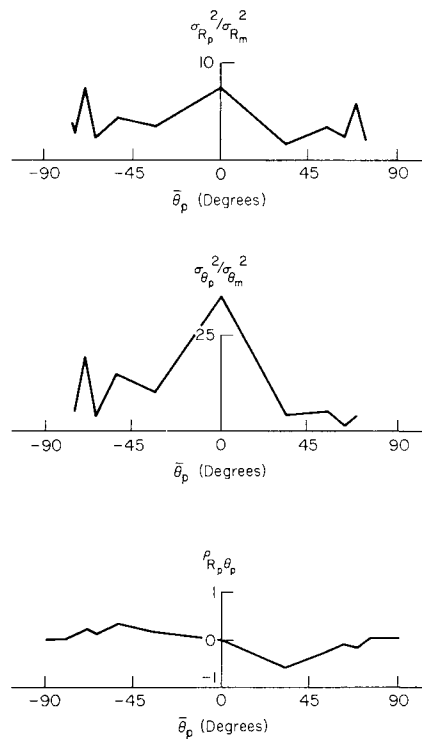


Fig. 5.7—Covariances of predicted range and azimuth for straight-line target trajectory $\bar{X}_m = 30$ n.mi., $v = 2000$ ft/s, $T = 4$, $\alpha = 0.56$, $\beta = 0.85$, for fade sequence (10001000100....)

Fig. 5.8—Covariances of predicted range and azimuth for straight-line target trajectory $\bar{X}_m = 2$ n.mi., $v = 2000$ ft/s, $T = 4$, $\alpha = 0.56$, $\beta = 0.85$, for fade sequence (10001000100....)



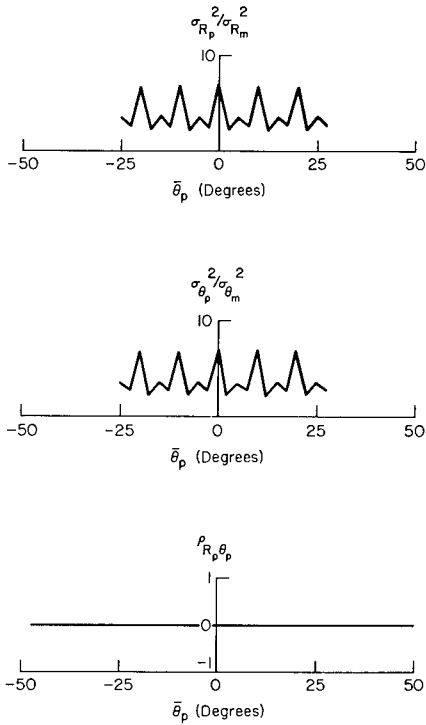


Fig. 5.9—Covariances of predicted range and azimuth for a filter in polar coordinates operating under fading conditions (1000100010...), $\alpha = 0.56$, $\beta = 0.85$

Fig. 5.10—Covariances of predicted range and azimuth for circular flight path $\bar{R}_m = 21.2$ n.mi., $\theta_m = 45^\circ$, $v = 2000$ ft/s, $T = 4$ s, 3-g turn, $\alpha = 0.56$, $\beta = 0.85$, under fading conditions (10001000100...), (X-Y) track

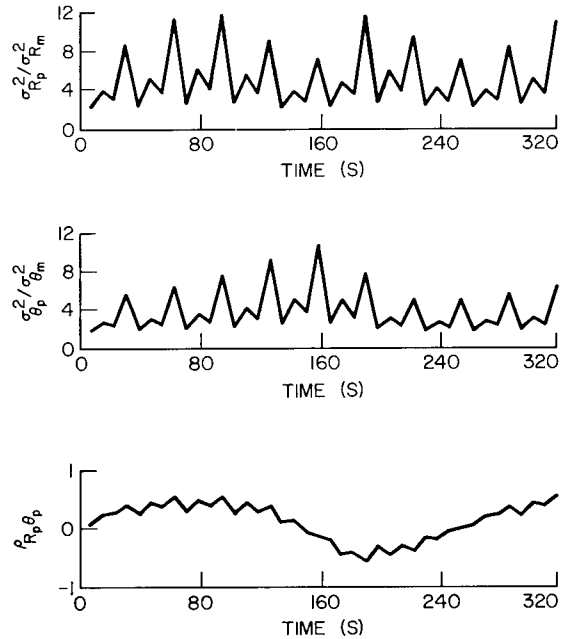


Fig. 5.11—Covariances of predicted range and azimuth for circular flight path $\bar{R}_m = 210.2$ n.mi., $\bar{\theta}_m = 45^\circ$, $v = 2000$ ft/s, $T = 4$ s, 3-g turn, $\alpha \times 0.56$, $\beta = 0.85$, under fading conditions (1000100010...), (X-Y) track

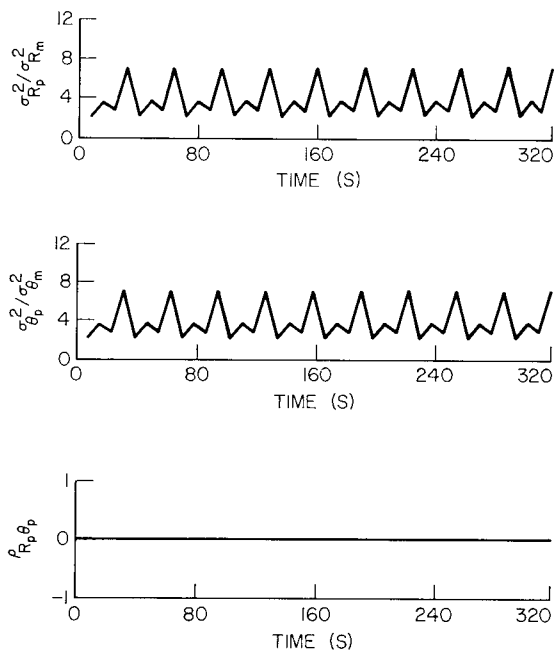
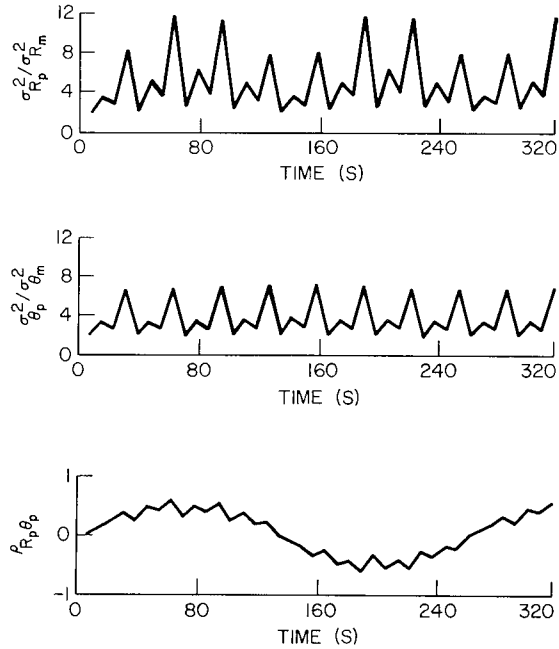


Fig. 5.12—Covariances of predicted range and azimuth for a filter in polar coordinates operating under fading conditions (10010010...), $\alpha = 0.56$, $\beta = 0.85$

5.3 Track Handoff Problem

In this section, the abilities of the polar and cartesian α - β filters to perform the track handoff problem are compared. Since the details of the track handoff simulation are given in Ref. 2, only the basic facts will be presented here.

The geometry of the situation is shown in Fig. 5.13. The coordinates of the target at time $t = 0$ are (x_0, y_0, h_0) , its height when crossing the y axis is h_f , its ground speed is v , and its heading is A . The radar coordinates are $(0, 0, h_r)$.

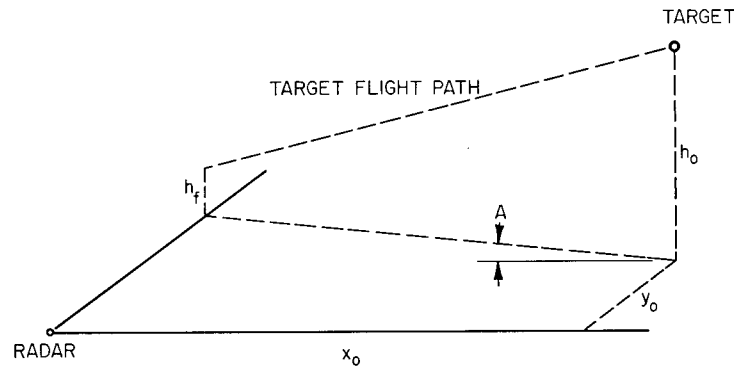


Fig. 5.13—Geometry of radar and target

The simulation is run in the following manner: The target is assumed to be detected on every scan of the search radar. Initially, three target positions are generated, and the α - β filter is initialized. After each additional detection, the α - β filter is updated and is used to continuously estimate the target's coordinates. Starting with the third sample, the center of the tracking scan pattern is centered on the predicted position of the target. The search pattern of the tracking radar is initialized, and during each update time, the program calculates whether or not the target is located within the acceptance beam of the tracking radar (Section 5.4). The simulation continues until the target crosses the y axis. The output of a single case is a series of correct and incorrect handoffs between the search and tracking radars. Many cases are runs, and the probability of handing off as a function of range is estimated.

The initial simulation was run with the following target parameters: x_0 was uniformly distributed between 121,600 ft (20 n.mi.) and 122,600 ft, $y_0 = 0$, $h_0 = 10,000$ ft, $h_f = 5000$ ft, Δ is uniformly distributed between 5.9° and 6.1° ,* and V is uniformly distributed between 2100 and 2300 ft/s. The radar is at a height of 80 ft, has a range resolution of 250 ft and a scanning rate (update time) of 4 s, and measures the azimuth position with a standard deviation of 0.5° . The deviation accuracy of the radar will be varied in the simulation. It will have a standard deviation of 1° , or else the radar (a 2-D radar) assumes that the elevation of the target is always 12° (the bottom of the 24° scan pattern of the tracking radar is set on the horizon). The filter parameters are $\alpha = 0.6$ and $\beta = 0.9$ for range, $\alpha = \beta = 0.5$ for azimuth, and $\alpha = 0.56$ and $\beta = 0.85$ for X and Y .

*This makes the target pass within 2 mi of the radar.

For each of the two elevation accuracies and two filters, 50 cases were run; and the probability of the target being in the beam of the tracking radar on the last scan pattern, vs the target range, is shown in Figs. 5.14 and 5.15. It is obvious that one can hand off targets at closer ranges using the X-Y filter. This is because of the large accelerations in the $R-\theta$ coordinate system for crossing targets.

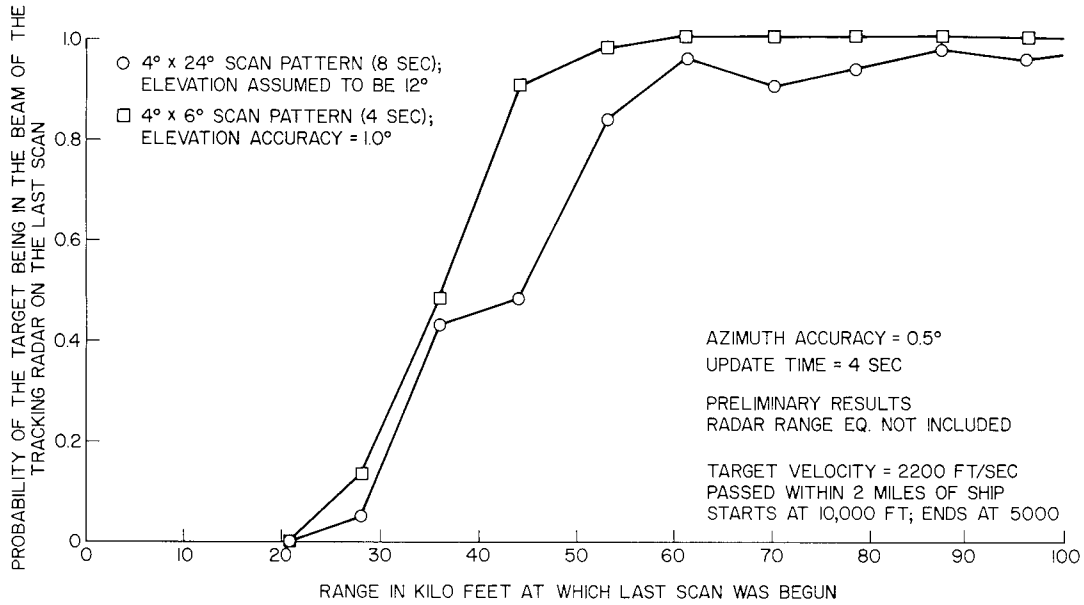


Fig. 5.14—Probability of handoff using $R-\theta$ filter

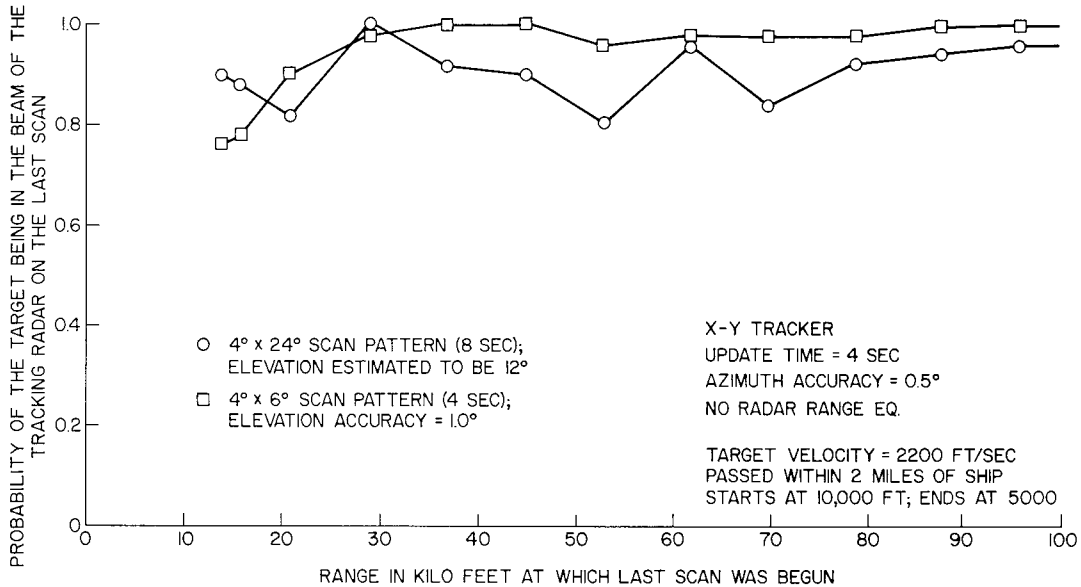


Fig. 5.15—Probability of handoff using X-Y filter

5.4 Discussion of Results

The mean errors in the polar and cartesian filters were found to increase during fades unless the target was moving at a constant velocity along the polar or cartesian coordinates, respectively. For short fades at the longer ranges, there seemed to be very little difference between the mean errors in either system. The covariances increased during fading conditions.

One can hand off targets at closer ranges using the X - Y filter. This is because of the large accelerations in the R - θ coordinate system for crossing targets.

6.0 CONCLUSION

This report describes an approximate analytical procedure for determining the errors in an α - β filter operating in cartesian coordinates. These errors are separated into mean and covariance errors and are compared to the errors in an α - β filter operating in polar coordinates.

The polar to cartesian and cartesian to polar coordinate transformations are shown to be approximately linear over the space in which the central and near tail regions of the probability density lie. Since the measurement probability density is Gaussian, it is shown that the probability densities after the transformations can be approximated with a high degree of accuracy with Gaussian densities as long as the far tail region is of little concern. Using this result, we find the covariances at the output of the filters. Closed-form steady-state solutions are found for the covariances in the polar coordinate filter and for stationary targets using the cartesian coordinate filter. These covariances depend upon α , β , and measurement variances. For moving targets, the cartesian coordinate filter yields output covariances which are nonstationary. Their values depend upon α , β , measurement variances, target trajectory, target speed, and sampling time. In steady state and for the far ranges, the output variances using the cartesian coordinate filter approach the variances obtained from the polar coordinate filter. At the near ranges, the covariances are in general larger in the cartesian coordinate filter as compared to the polar coordinate filter.

At the far ranges the mean errors using either filtering system are essentially the same. But at the close ranges the mean error in the polar coordinate system is in general larger than in the cartesian coordinate filter.

In the study on the effects of short fades using the predicted target strategy, it was generally found that both the mean errors and covariances increased during the time of the fade.

In the study of the track handoff problem it was found that one could hand off targets at closer ranges using the X - Y filter. This is because of the large accelerations in the R - θ coordinate system for crossing targets.

ACKNOWLEDGMENT

I would like to thank Dr. G. V. Trunk for discussing the problems involved in this report with me and for contributing the results shown in Section 5.3.

REFERENCES

1. B. H. Cantrell, "Behavior of α - β Tracker for Maneuvering Targets Under Noise, False Target, and Fade Conditions," NRL Report 7434, Aug. 17, 1972
2. B. H. Cantrell and G. V. Trunk, "Analysis of the Track Handoff Between the Search and Track Radars," NRL Report 7505, Dec. 29, 1972
3. J. T. Tou, *Digital and Sampled-Data Control Systems*, 1st ed., McGraw Hill, New York, 1959
4. J. S. Meditch, *Stochastic Optimal Linear Estimation and Control*, 1st ed., McGraw Hill, New York, 1969

Appendix
CALCULATION OF MEANS AND COVARIANCES OF RADAR
MEASUREMENTS IN TERMS OF CARTESIAN COORDINATES

A radar measurement is given in range R and azimuth θ , where R and θ are assumed to be uncorrelated, Gaussian-distributed random variables with means $\bar{\theta}$ and \bar{R} , and variances σ_R^2 and σ_θ^2 . The problem is to determine the means and covariances of the two quantities X and Y defined as

$$X = R \cos \theta \quad (\text{A1})$$

$$Y = R \sin \theta . \quad (\text{A2})$$

In the calculations the following two facts are used extensively. The approximation

$$e^{-2\sigma_\theta^2} = 1 + \sum_{N=1}^{\infty} \frac{(-2\sigma_\theta^2)^N}{N!} \approx 1 - 2\sigma_\theta^2 \quad (\text{A3})$$

is used because the azimuth standard deviation σ_θ in radians found in typical search radars is small. The integral

$$\int_0^{\infty} e^{-\alpha^2 X^2} \cos bX \, dX = \frac{\sqrt{\pi} e^{-b^2/4\alpha^2}}{2\alpha}, \quad \text{where } \alpha > 0 \quad (\text{A4})$$

is used in each of the calculations.

The major steps in the calculations are the following.

Mean of X , \bar{X}

$$\bar{X} = E[R] E[\cos \theta] \quad \text{where } E[R] = \bar{R}$$

$$E[\cos \theta] = \frac{1}{\sqrt{2\pi} \sigma_\theta} \int_{-\infty}^{\infty} \cos \theta e^{-(1/2)[(\theta-\bar{\theta})/\sigma_\theta]^2} d\theta .$$

Change of variable $\omega = \theta - \bar{\theta}$

$$E[\cos \theta] = \frac{1}{\sqrt{2\pi} \sigma_\theta} \int_{-\infty}^{\infty} [\cos \omega \cos \bar{\theta} - \sin \omega \sin \bar{\theta}] e^{(-1/2)(\omega/\sigma_\theta)^2} d\omega$$

$$E[\cos \theta] = \frac{2 \cos \bar{\theta}}{\sqrt{2\pi} \sigma_\theta} \int_0^\infty \cos \omega e^{-(1/\sqrt{2} \sigma_\theta)^2 \omega^2} d\omega$$

$$E[\cos \theta] = e^{-\sigma_\theta^2/2} \cos \bar{\theta}$$

$$\bar{X} = \bar{R} e^{-\sigma_\theta^2/2} \cos \bar{\theta}; \quad \text{for small } \sigma_\theta, \quad \bar{X} = \bar{R} \cos \bar{\theta} \quad \text{Eq. (2.13)}$$

Mean of Y , \bar{Y}

Similar to calculation of \bar{X}

$$\bar{Y} = \bar{R} e^{-\sigma_\theta^2/2} \sin \bar{\theta}; \quad \text{for small } \sigma_\theta, \quad \bar{Y} = \bar{R} \sin \bar{\theta} \quad \text{Eq. (2.14)}$$

Variance of X , $\text{VAR } X$

$$\text{Var } X = E[X^2] - (E[X])^2 = E[R^2] E[\cos^2 \theta] - \bar{X}^2$$

$$E[\cos^2 \theta] = \frac{1}{\sqrt{2\pi} \sigma_\theta} \int_{-\infty}^\infty \cos^2 \theta e^{-(1/2)[(\theta-\bar{\theta})/\sigma_\theta]^2} d\theta$$

$$E[\cos^2 \theta] = \frac{1}{2} \times \frac{1}{\sqrt{2\pi} \sigma_\theta} \int_{-\infty}^\infty e^{-(1/2)[(\theta-\bar{\theta})/\sigma_\theta]^2} d\theta \\ + \frac{1}{2} \times \frac{1}{\sqrt{2\pi} \sigma_\theta} \int_{-\infty}^\infty \cos 2\bar{\theta} e^{-(1/2)[(\theta-\bar{\theta})/\sigma_\theta]^2} d\theta.$$

Let $\omega = \theta - \bar{\theta}$;

$$E[\cos^2 \theta] = \frac{1}{2} + \frac{1}{2} \times \frac{1}{\sqrt{2\pi} \sigma_\theta} \int_{-\infty}^\infty \cos (2\omega + 2\bar{\theta}) e^{(-1/2)(\omega/\sigma_\theta)^2} d\omega$$

$$E[\cos^2 \theta] = \frac{1}{2} + \frac{1}{2} \times \frac{1}{\sqrt{2\pi} \sigma_\theta} \int_{-\infty}^\infty (\cos 2\omega \cos 2\bar{\theta} - \sin 2\omega \sin 2\bar{\theta}) \\ \times e^{(-1/2)(\omega/\sigma_\theta)^2} d\omega$$

$$E[\cos^2 \theta] = \frac{1}{2} + \frac{2 \cos 2\bar{\theta}}{2 \sqrt{2\pi} \sigma_\theta} \int_{-\infty}^\infty \cos 2\omega e^{-(1/\sigma_\theta \sqrt{2})^2 \omega^2} d\omega$$

$$E[\cos^2 \theta] = \frac{1}{2} + \frac{1}{2} e^{-2\sigma_\theta^2} \cos 2\bar{\theta}$$

$$E[R^2] = \sigma_R^2 + (\bar{R})^2$$

$$\text{Var } X = E[R^2] E[\cos^2 \theta] - (\bar{X})^2; \quad \text{for small } \sigma_\theta,$$

$$\text{Var } X = \sigma_R^2 \cos^2 \bar{\theta} + (\bar{R})^2 \sigma_\theta^2 \sin^2 \bar{\theta} \quad \text{Eq. (2.10)}$$

Variance of Y, Var Y

Similar to calculation of Var X, for small σ_θ ,

$$\text{Var } Y = \sigma_R^2 \sin^2 \bar{\theta} + (\bar{R})^2 \sigma_\theta^2 \cos^2 \bar{\theta}. \quad \text{Eq. (2.11)}$$

Covariance of X and Y, Cov XY

$$\text{cov } XY = E[XY] - E[X] E[Y] = E[R^2] E[\cos \theta \sin \theta] - \bar{X} \bar{Y}$$

$$E[\cos \theta \sin \theta] = \frac{1}{2} \times \frac{1}{\sqrt{2\pi} \sigma_\theta} \int_{-\infty}^{\infty} \sin 2\theta e^{-(1/2)[(\theta-\bar{\theta})/\sigma_\theta]^2} d\theta$$

$$\omega = \theta - \bar{\theta}$$

$$E[\cos \theta \sin \theta] = \frac{1}{2\sqrt{2\pi} \sigma_\theta} \int_{-\infty}^{\infty} (\sin 2\omega \cos 2\bar{\theta} + \cos 2\omega \sin 2\bar{\theta}) e^{-(1/2)(\omega/\sigma_\theta)^2} d\omega$$

$$E[\cos \theta \sin \theta] = \frac{\sin 2\bar{\theta}}{\sqrt{2\pi} \sigma_\theta} \int_{-\infty}^{\infty} \cos 2\omega e^{-(1/\sigma_\theta \sqrt{2})^2 \omega^2} d\omega$$

$$E[\cos \theta \sin \theta] = \frac{1}{2} e^{-2\sigma_\theta^2} \sin 2\bar{\theta}$$

$$E[R^2] = \sigma_R^2 + (\bar{R})^2$$

$$\text{cov } XY = E[R^2] E[\cos \theta \sin \theta] - \bar{X} \bar{Y}; \quad \text{for small } \sigma_\theta,$$

$$\text{cov } XY = \frac{\sigma_R^2}{2} \sin 2\bar{\theta} - \frac{\bar{R} \sigma_\theta^2}{2} \sin 2\bar{\theta}. \quad \text{Eq. (2.12)}$$